The mass distribution function of cosmic nonlinear structures
Lee, Jounghun
ProQuest Dissertations and Theses; 1999; ProQuest

INFORMATION TO USERS

This manuscript has been reproduced from the microfilm master. UMI films the text directly from the original or copy submitted. Thus, some thesis and dissertation copies are in typewriter face, while others may be from any type of computer printer.

The quality of this reproduction is dependent upon the quality of the copy submitted. Broken or indistinct print, colored or poor quality illustrations and photographs, print bleedthrough, substandard margins, and improper alignment can adversely affect reproduction.

In the unlikely event that the author did not send UMI a complete manuscript and there are missing pages, these will be noted. Also, if unauthorized copyright material had to be removed, a note will indicate the deletion.

Oversize materials (e.g., maps, drawings, charts) are reproduced by sectioning the original, beginning at the upper left-hand corner and continuing from left to right in equal sections with small overlaps. Each original is also photographed in one exposure and is included in reduced form at the back of the book.

Photographs included in the original manuscript have been reproduced xerographically in this copy. Higher quality 6" x 9" black and white photographic prints are available for any photographs or illustrations appearing in this copy for an additional charge. Contact UMI directly to order.

UMI®

Bell & Howell Information and Learning
300 North Zeeb Road, Ann Arbor, MI 48106-1346 USA
800-521-0600

Reproduced with permission of the copyright owner. Further reproduction prohibited without permission.

Reproduced with permission of the copyright owner. Further reproduction prohibited without permission.

The Mass Distribution Function of Cosmic Nonlinear Structures

by

Jounghun Lee
B.S., Korea University, 1993

Submitted to the Department of Physics and Astronomy
and the Faculty of the Graduate School of the University
of Kansas in partial fulfillment of the requirements for
the degree of Doctor of Philosophy

Sergei F. Shandarin, Professor of Physics & Astronomy, Faculty Advisor

Hume A. Feldman, Assistant Professor of Physics & Astronomy

Raymond G. Ammar, Professor of Physics & Astronomy

Nowhan Kwak, Professor of Physics & Astronomy

Glen B. Leimkuhler, Professor of Mathematics

2-12-99
Date Defended

Diss
1999
L442
(Archives)

R00331 72789

MAY 23 1999

Reproduced with permission of the copyright owner. Further reproduction prohibited without permission.

UMI Number: 9946108

UMI Microform 9946108
Copyright 1999, by UMI Company. All rights reserved.

This microform edition is protected against unauthorized
copying under Title 17, United States Code.

UMI
300 North Zeeb Road
Ann Arbor, MI 48103

Reproduced with permission of the copyright owner. Further reproduction prohibited without permission.

Abstract

Jounghun Lee, Ph.D.
Department of Physics & Astronomy, 1999
University of Kansas

To understand the formation of large-scale structure, it is desirable to have an analytical framework within which theoretical predictions for structure formation can be made. Press-Schechter (PS) pioneered this field and proposed an analytical formalism for the cosmological mass distribution function with the top-hat spherical model as an underlying dynamics. Although the PS mass function has so far provided an effective analytical tool to study the structure formation, recent numerical experiments have shown the limitation of the PS theory. In this thesis I develop a new analytical formalism to evaluate the mass function by extending the PS theory to a realistic nonspherical dynamical model where the Zel'dovich approximation is chosen as a guiding dynamics. I compare the resulting new mass function with numerical data from high resolution N-body simulations, and show that the new mass function agrees with the numerical data much better than the PS mass function.

As an application of the mass function theory, I also investigate the large scale biasing effect of the primordial gravitational potential on the formation of galaxy-clusters. By incorporating the potential terms into the mass function, I measure the biasing effect quantitatively for the case of a cold dark matter model and show that galaxy clusters are not distributed randomly but strongly biased towards the troughs of the potential with characteristic scale of $120h^{-1}$Mpc.

Reproduced with permission of the copyright owner. Further reproduction prohibited without permission.

To Taiji ...

Reproduced with permission of the copyright owner. Further reproduction prohibited without permission.

Acknowledgments

First of all I thank God and my lord Jesus Christ whom I praise and glorify through this work. I thank my parents who always pray for me and support me emotionally. I thank my advisor Dr. Sergei Shandarin for his teaching and academic support. I also thank Drs. Hume Feldman and Douglas Mckay for their thoughtful advice and councelling. Thanks to Dr. Herman Munczek who showed me a paragon of best not only in professorship but also in humanity. Thanks to Drs. Raymond Ammar and Babara Anthony Twarog who protected me when I experienced the most difficult times. Thanks to Drs. Bepi Tormen and Fabio Governato who kindly provided their numerical data to me. Thanks to Dr. Nowan Kwak, Dr. Bob Dinsdale and Katherine Dinsdale who gave me a ride to church and strenghtened me through their faith. Thanks to Sheryl Henry and Fumiko Shil whose friendships and warm hearts brightened my days. Thanks to my aunt Dr. Kung Sook Lee who has always taken care of my health. Thanks to my undergraduate teachers Drs. Sun Hee Kwun and Chul E Lee who encouraged me to go for Ph.D. in physics. Thanks to my ex officemates Drs. Capp Yess and Jennifer Pauls who were willing to correct my English and helped me adjust to American culture.

Finally, I wish to give my special thanks to Taiji Seo (my pure Adonis) without whom and whose music it would have been impossible.

Reproduced with permission of the copyright owner. Further reproduction prohibited without permission.

Contents

Reproduced with permission of the copyright owner. Further reproduction prohibited without permission.

Reproduced with permission of the copyright owner. Further reproduction prohibited without permission.

List of Figures

Reproduced with permission of the copyright owner. Further reproduction prohibited without permission.

Reproduced with permission of the copyright owner. Further reproduction prohibited without permission.

Reproduced with permission of the copyright owner. Further reproduction prohibited without permission.

List of Tables

Reproduced with permission of the copyright owner. Further reproduction prohibited without permission.

Chapter 1

Overview: Cosmological Studies of the Large-Scale Structure of the Universe

1.1 Introduction

Our present universe is observed to be quite clumpy with numerous galaxies, groups of galaxies (5-100 galaxies), galaxy clusters (more than 100 galaxies) and etc., which span a large dynamic range in mass (typical mass in a galaxy $\sim 10^{12} M_{\odot}$, while $\sim 10^{14} - 10^{15} M_{\odot}$ for a galaxy cluster [1]). One of the most fundamental problems in cosmology is to understand the formation and the evolution of this large-scale structure of the universe.

Rapid increase and progress in observational discoveries and theoretical insights of the past two decades has given birth to an elegant scenario which enables us to understand the basic mechanism for structure formation. According to this, what is called, gravitational instability scenario, the universe, starting from its

[1] There are three different ways to estimate cluster masses. One is by applying the virial theorem to the positions and the velocities of galaxies, another is by X-ray analysis, and the other is by gravitational lensing effect (Lewis et al. 1999)

Reproduced with permission of the copyright owner. Further reproduction prohibited without permission.

fiery origin – the Big Bang, was initially homogeneous but had some small density fluctuations with a characteristic spectrum. As the universe evolves, density fluctuations were amplified and concentrated via gravitational instability, which eventually led to the formation of cosmic structures that we observe today.

Most of current theories aiming at more detailed and quantitative description of structure formation are based on this general idea. In this introductory Chapter, we review the standard model of structure formation on which the topic of this thesis–the mass function theory is based.

1.2 The Evolving Universe

1.2.1 The Hot Big Bang

Since 1920's, it has been known (Hubble 1929) that the emission light from distant galaxies are redshifted, and the more distant galaxies are from the Milky way, the bigger the amount of redshift $z \equiv (\lambda - \lambda_0)/\lambda_0$ (λ: the observed wavelength, λ_0: the original wavelength) is. This observational fact directly indicates that each galaxy is receding from one another at a speed proportional to its distance from our galaxy. In other words the universe is expanding. The expansion rate of the present universe is quantified by the Hubble constant, H_0:

$$H_0 = 100h \,\mathrm{km\,s^{-1}\,Mpc^{-1}}, \tag{1.1}$$

with the uncertainty $0.53 \leq h \leq 0.68$ (Sandage 1999).

Turning a clock backwards from the present time, we can infer that the universe in its very early epoch must have been very small in size compared with the present, so incredibly dense and hot, consisting mostly of radiation. As the universe expands, its temperature has fallen down. This picture which revolutionized the twentieth-century cosmology is called the "Hot Big Bang".

Reproduced with permission of the copyright owner. Further reproduction prohibited without permission.

The most convincing evidence supporting the Big Bang model is the cosmic microwave background radiation (CMBR) discovered by Penzias and Wilson in 1964. The Big Bang theory predicts that if the universe has evolved from a hot and dense beginning, then it should now possess a cooled down remnant of radiation background. The very existence of CMBR and almost perfect match of its thermal spectrum with the theoretical prediction place the Hot Big Bang at the level of "standard" cosmological model (Lubin & Villela 1985; Smoot 1999).

Another compelling observational data which stand by the Big Bang model are the observed abundances of light elements, deuterium (^2H), helium (^3He), and lithium (^7Li). The abundances of all heavier elements than these light ones in the universe can be explained in terms of stellar nucleosynthesis. But there are much more ^2H, ^3He, ^7Li present in the universe than could be explained by the stellar nucleosynthesis.

The Big Bang model provides a refined solution to this astronomical puzzle. In the Big Bang model cosmic primordial nucleosynthesis produced these light elements when the universe was about 1 minute old. What the detailed calculations of the Big Bang theory predicts turned out to be in good accord with the observed abundances of the light elements (Pagel 1991). In addition, one condition claimed for explaining the light element abundances by the Big Bang model that there should be no more than three types of neutrinos obtained a experimental confirmation recently (Adeva et al. 1989).

1.2.2 Relativistic Universe

Einstein's general relativity has provided a noble framework within which the Hot Big Bang can be described in terms of mathematical equations. The geometry of the spacetime of an expanding homogeneous and isotropic universe is described

Reproduced with permission of the copyright owner. Further reproduction prohibited without permission.

by the following Friedmann-Robertson- Walker (FRW) line element:

$$ds^2_{FRW} = c^2dt^2 - a^2(t)\left[\frac{dr^2}{1-\kappa r^2} + r^2d\theta^2 + r^2\sin^2\theta d\phi^2\right], \qquad \kappa = 0, \pm 1, \quad (1.2)$$

where κ is a curvature constant such that $\kappa = 0, -1, +1$ correspond to flat (Euclidean), open (hyperbolically curved), closed (spherically curved) spacetime respectively. For a FRW universe filled with a perfect fluid which is in fact a good approximation to the early universe in the Big Bang model, the Einstein field equations are reduced to the following fundamental equations of cosmology:

$$H^2(t) = \left(\frac{\dot{a}}{a}\right)^2 = \frac{8\pi G}{3}\rho + \frac{\Lambda}{3} - \frac{\kappa c^2}{a^2}, \quad (1.3)$$

$$\frac{\ddot{a}}{a} = -\frac{4\pi G}{3c^2}\left(\rho c^2 + 3p\right) + \frac{\Lambda}{3}. \quad (1.4)$$

Here $a(t)$ is the expansion parameter related to the Hubble parameter $H(t)$ by $\dot{a(t)}/a(t) \equiv H(t)$ describing how fast the universe expands, ρ and p are the mass density and the pressure of the fluid respectively, and Λ is the cosmological constant representing the vacuum energy of the universe. With the usual assumption of $\Lambda = 0$ (this assumption will be used throughout this paper), $\kappa = 0$ leads to $H^2 = 8\pi G\rho/3$ by equation (1.3). The corresponding energy density $3H^2/8\pi G$ is called the *critical density* and denoted as ρ_c.

In forecasting the destiny of the universe, it is useful to define the density parameter $\Omega \equiv \rho/\rho_c$. If $\Omega < 1$ ($\kappa = -1$), then the universe is open, so will expand for ever; if $\Omega = 1$ ($\kappa = 0$) , the universe is flat, still will expand for ever but at a slower rate than the $\Omega < 1$ universe; if $\Omega > 1$ ($\kappa = 1$), then the universe is close, so will stop expanding at some time in the future, and then will start contracting.

The true value of Ω has not been determined yet, and depends on how much dark matter the universe has. Dark matter refers to the invisible matter present in the universe whose existence can be detected only by its gravitational effect on

Reproduced with permission of the copyright owner. Further reproduction prohibited without permission.

its surrounding. It is believed that the energy density of the universe is dominated by dark matter mostly in a form of nonbaryonic elementary particles although its nature has not been known to us yet (e.g., Gelmini 1990).

Observational cosmologists by far have found Ω to be in the range of 0.3 ± 0.1, much less than unity (e.g., Fan, Bahcall, & Cen 1997), whereas theoretical cosmologists favor $\Omega = 1$ flat universe. Especially the current popular inflation scenario predicts that our universe must be flat. Inflation scenario proposed by Guth in 1981 states that the universe should undergo a huge, rapidly accelerating expansion at the cosmic age of between 10^{-43} and 10^{-32} second. Although inflation is still a postulate waiting for observational tests, it is an attractive concept since it has been shown that several long-standing cosmological problems can be solved by the inflation theory in the Big Bang framework (see Linde 1990 for a detailed description of the inflation model).

1.2.3 Cosmic History

One of the most unique features of the Big Bang model is that the history of the universe is broadly divided into two strikingly different eras: the radiation-dominated era and the matter-dominated era.

During the radiation-dominated era (corresponding to the first million years) when the universe was extremely hot and dense, matter could not exist in the form of electrically neutral atoms. Matter was ionized, electrons being separated from nuclei (i.e., protons). And the electromagnetic radiation (i.e., photons) were strongly coupled with this ionized relativistic matter via its continual collisions with free electrons. Consequently photons could not propagate freely, so the universe was opaque, and matter were not able to condense out structures. Thus with matter and radiation in equilibrium maintaining the same temperature, the dynamics of the universe at this era was mostly determined by radiation and the energy density of the universe varied as $\rho(t) \propto a^{-4}(t)$ since radiation experiences

Reproduced with permission of the copyright owner. Further reproduction prohibited without permission.

both the volume expansion varied as a^{-3} and the redshift varied as a^{-1}.

As the universe cooled down through its expansion, free electrons and nuclei began to be recombined, forming neutral atoms. Decrease in the abundances of free electrons resulted in decrease in the frequency of the collisions between photons and electrons. In other words, matter and radiation began to be decoupled from each other.

The complete cessation of the coupling between matter and radiation occurred when the temperature of the universe fell below $T_{rec} \sim 4000$K (corresponding to $z \sim 1500$). Electrons were all recombined to protons (hydrogen recombination), and photons propagated freely into all directions. Thereafter matter and radiation without interacting with each other evolved into separate histories.

As for the decoupled radiation, the only interference it experienced afterwards was the cosmic expansion which caused radiation temperature to fall simply as follows:

$$T(t) = T_{rec}\frac{1+z}{1+z_{rec}}. \tag{1.5}$$

With the above given temperature, the radiation after decoupling has maintained a black body distribution which we can observe today as CMBR. The present temperature of CMBR according to the most recent measurement carried out with the American satellite COBE (COsmic Background Explorer) gives the value of $T_0 = 2.7377 \pm 0.0038$ (Smoot 1999).

The matter-dominated era which lasts till the present epoch started after the matter-radiation equilibrium ($z_{eq} \approx 5,000$: the instant in time when contributions of matter and radiation on the dynamics of universe are the same) After recombination the universe became transparent, consequently clumpy structures like galaxies, stars, and so forth has appeared. In the next section we study how these structures formed and how they have evolved.

But before closing this section, let us estimate the age of the universe under some simplified assumptions. Since the radiation dominated era occupied only a

Reproduced with permission of the copyright owner. Further reproduction prohibited without permission.

short period of time, we can consider only the matter-dominated universe with $\Lambda = 0$, $\Omega = 1$ which case we will focus on throughout this thesis. The energy density $\rho(t)$ of the universe dominated by matter falls in proportional to $a^{-3}(t)$ due to the cosmic expansion:

$$\rho(t) = \rho_0(t)\left(\frac{a_0}{a}\right)^3. \tag{1.6}$$

The Friedmann equation (1.3) with $p = 0$ (radiation pressure is negligible in the matter dominated universe) along with equation (1.6) and $\rho_c = 3H^2/8\pi G$ (see §1.2.2) gives us

$$a(t) = a_0\left(\frac{t}{t_0}\right)^{2/3}, \qquad t_0 = \frac{2}{3H_0}, \tag{1.7}$$

where a_0, t_0 and H_0 are the cosmic expansion factor, the age of the universe, and the Hubble constant respectively at the present epoch. Plugging the approximate value of $H_0 = 100\,h$ km s^{-1} Mpc^{-1} into equation (1.7), one has

$$t_0 \approx 6.5h^{-1}\text{Gyr}, \tag{1.8}$$

which sets an upper limit for the age of $\Omega = 1$ universe. But this upper limit on the age of our universe disagrees with recent astronomical measurements: Atronomers believe that they found the oldest stars at the age of 15Gyr (Lachieze-Rey 1995), which implies that the value of Ω must be less than unity , or the cosmological constant Λ must be nonzero [2].

1.3 Structure Formation

As mentioned in § 1.2.2, the collisionless dark matter dominates the mass density of the universe. According to its nature, the dark matter is categorized into

[2]Recently a nonzero cosmological model has been invoked to reconcile the age of our universe with $\Omega = 1$ universe where now $\Omega = \Omega_\Lambda + \Omega_{matter}$ at present epoch.

Reproduced with permission of the copyright owner. Further reproduction prohibited without permission.

the "hot" and the "cold". The hot dark matter decoupled while they were still relativistic, so has a tendency to have high velocity dispersion. Whereas the cold dark matter has low velocity dispersion since it was nonrelativistic at the time of decoupling.

The standard hierarchical clustering theory adopts the cold dark matter model. It states that due to the small velocity dispersion of the cold dark matter, stars first form to produce small structures of galaxy size, and then agglomeration of these small structures leads to the formation of larger structures like galaxy clusters.

The small amplitude density perturbations which are assumed to originate from the quantum process during the inflation phase (Efstathiou 1990) grow, recollapse and eventually form the dark halos under the influence of gravity in the hierarchical way. The virialized halos of dark matter produce gravitational potential wells where gas condenses into stars to form luminous galaxies. Subsequently groups and clusters of galaxies form by the merging of the galaxies bound to a common dark halos.

The perturbed FRW universe can be described by the following line element:

$$ds^2 = ds^2_{FRW} + h_{ij}dx^i dx^j, \qquad i,j = 1,2,3, \tag{1.9}$$

where h_{ij} represents the amplitude of the perturbations. In the linear limit of $h_{ij}h^{ij} \ll 1$ with the assumption that the length scale of the perturbations is much smaller than the horizon scale and that the mean free path of a particle is small, the following set of three Newtonian equations for a perfect fluid governs the dynamics of the dark matter:

The *continuity* equation:

$$\frac{\partial \delta}{\partial t} + \frac{1}{a}\nabla_{\mathbf{x}} \cdot [(1+\delta)\mathbf{v}] = 0. \tag{1.10}$$

Reproduced with permission of the copyright owner. Further reproduction prohibited without permission.

The *Euler* equation:

$$\frac{\partial \mathbf{v}}{\partial t} + \frac{\dot{a}}{a}\mathbf{v} + \frac{1}{a}(\mathbf{v}\cdot\nabla_{\mathbf{x}})\mathbf{v} + \frac{c_s^2}{a}\nabla_{\mathbf{x}}\delta + \frac{1}{a}\nabla_{\mathbf{x}}\varphi = 0. \tag{1.11}$$

The *Poisson* equation:

$$\nabla_{\mathbf{x}}^2\varphi = 4\pi G\bar{\rho}a^2\delta. \tag{1.12}$$

Here $\mathbf{x} \equiv \mathbf{r}/a$ ($\mathbf{r}$: the proper coordinate) is the comoving coordinate, $\mathbf{v} \equiv a\dot{\mathbf{x}}$ is the peculiar velocity – the velocity with respect to the comoving coordinate, $\delta(\mathbf{x},t) \equiv \Delta\rho(\mathbf{x},t)/\bar{\rho}(t)$ is the dimensionless density contrast ($\bar{\rho}$: the mean mass density of the universe), $\varphi(\mathbf{x},t)$ is the gravitational potential, and c_s is the speed of sound.

In the following two subsections, we find an approximate solution to the above equations using the linear perturbation theory and study statistical properties of the initial density perturbations.

1.3.1 Linear Perturbation Theory

The first order perturbation theory enables us to obtain an approximate solution to the above set of three nonlinear equations (Peebles 1990). Expanding the density , the velocity, the potential terms into $\delta(\mathbf{x}) \approx \delta_0 + \delta_L(\mathbf{x},t), v(\mathbf{x}) \approx \mathbf{v}_0 + \mathbf{v}_L(\mathbf{x},t), \varphi(\mathbf{x}) \approx \varphi_0 + \varphi_L(\mathbf{x},t)$, keeping only the first order terms, and dropping the pressure term in equations (1.10)–(1.12), we obtain a second order differential equation for the linearized $\delta_L(\mathbf{x},t)$:

$$\frac{\partial^2\delta_L}{\partial t^2} + 2H\frac{\partial\delta_L}{\partial t} - 4\pi G\bar{\rho}\delta_L = 0. \tag{1.13}$$

For a flat matter dominated universe, the mean mass density of the universe evolves as $\bar{\rho} = (6\pi G t^2)^{-1}$ according to equations (1.6) and (1.7). Inserting it into

Reproduced with permission of the copyright owner. Further reproduction prohibited without permission.

equation (1.13) gives the following general solution:

$$\delta_L(\mathbf{x},t) = \left[\frac{3}{5}\left(\frac{t}{t_i}\right)^{2/3} + \frac{2}{5}\left(\frac{t}{t_i}\right)^{-1}\right]\delta(\mathbf{x}). \tag{1.14}$$

This solutions shows that sixty percent of the initial amplitude grows as $t^{2/3}$ while the rest forty percent decays as t^{-1}. The growing mode of the solutions (say, $D_+ \propto t^{2/3}$) describes the gravitational growth of the initial density fluctuations $\delta(\mathbf{x})$ while the decaying mode ($D_- \propto t^{-1}$) describes the decrease of the fluctuations due to the cosmic expansion. Hence the structure formation corresponds only to the growing mode of the solution.

1.3.2 Statistical Description of the Density Perturbations

It is both impossible and meaningless to attempt to determine the exact value of $\delta(\mathbf{x})$ at any chosen point $\mathbf{x}$ since the exact initial conditions for $\delta(\mathbf{x})$ are not available. Rather the initial density perturbation $\delta(\mathbf{x})$ is regarded as a random field (i.e., $\delta(\mathbf{x})$ is a random variable at each $\mathbf{x}$) and its properties should be statistically determined by the probability distribution $p(\delta)d\delta$ which is often assumed to be Gaussian in the standard cosmology (Bardeen et al. 1986).

Often it is more convenient to work with its Fourier counterpart $\delta_{\mathbf{k}}$ than δ itself:

$$\delta_{\mathbf{k}} = \int_V \delta(\mathbf{x}) \exp(-i\mathbf{k}\cdot\mathbf{x}) d^3\mathbf{x}, \tag{1.15}$$

since in the $\mathbf{k}$-space $\delta_{\mathbf{k}}'s$ at different points evolve in approximately independent way while in the $\mathbf{x}$- space the effect of the gravity destroys very quickly the mutual independence among $\delta(\mathbf{x})'s$ at different points.

The two-point correlation function defined by

$$\begin{aligned} \xi(\mathbf{x}) &\equiv < \delta(\mathbf{x}')\delta(\mathbf{x}+\mathbf{x}') > \\ &= \int \frac{d^3k}{(2\pi)^3} |\delta_k|^2 \exp(i\mathbf{k}\cdot\mathbf{x}), \end{aligned} \tag{1.16}$$

Reproduced with permission of the copyright owner. Further reproduction prohibited without permission.

or its Fourier transform $|\delta_k|^2$ called the *power spectrum* characterizes the random field $\delta(\mathbf{x})$ completely. In other words, $\xi(\mathbf{x})$ or $|\delta_k|^2$ contains every statistical information about $\delta(\mathbf{x})$. For example, the mass variance (the rms density fluctuations) within a sphere of radius R can be obtained as

$$\sigma^2(M) = \int \frac{d^3k}{(2\pi)^3} |\delta_k|^2 W_k^2(R), \tag{1.17}$$

where $W(R)$ is a "filter" function introduced to average out the density fluctuations on scales less than the chosen scale R and M is the corresponding mass scale related to R by $M \propto \bar{\rho}R^3$ depending on the choice of a filter. The following three filters are most frequently used:

The *sharp k-space* filter:

$$W_k(R) = \Theta[2\pi/R - k], \qquad M = \frac{3}{4\pi}\bar{\rho}R^3, \tag{1.18}$$

The *top-hat* filter:

$$W_k(R) = \frac{3[\sin(kR) - kR\cos(kR)]}{(kR)^3}, \qquad M = \frac{4\pi}{3}\bar{\rho}R^3, \tag{1.19}$$

The *Gaussian* filter:

$$W_k(R) = \exp\left(-\frac{k^2}{2R^2}\right), \qquad M = (2\pi)^{3/2}\bar{\rho}R^3, \tag{1.20}$$

where Θ stands for the Heavyside step function.

1.4 Outline of the Upcoming Chapters

The theme of this thesis is the cosmological mass distribution function which gives the number densities of cosmic nonlinear structures at any specified mass range.

Chapter 2 reviews the classical mass function theory proposed by Press &

Reproduced with permission of the copyright owner. Further reproduction prohibited without permission.

Schechter in 1974. This review includes the underlying dynamical model, the statistical formalism, and the normalization problem of the Press-Schechter theory.

Chapter 3 introduces a new mass function theory which I have developed in collaboration with Sergei F. Shandarin. This new theory uses the Press-Shechter idea as its foundation but replaces the the unrealistic top-hat spherical model with the realistic nonspherical one based on the Zel'dovich approximation. I modify the Press-Schechter formula by implementing an anisotropic collapse condition, derive a new mass function using this new formula, find an approximate solution to the related normalization problem, and discuss the properties of the resulting mass function.

In Chapter 4 I compare the analytical mass functions with the numerical results derived from N-body simulations. I consider two fiducial initial spectrums, and show that the new mass function agrees with the N-body results much better than the PS one.

Chapter 5 is an application of the mass function theory. I investigate quantitatively the effect of the primordial gravitational potential on the structure formation by modifying the Press-Schechter formalism. With this modified technique, I derive two constrained mass functions which reveals the strong biasing in the formation of galaxy clusters due to the primordial gravitational potential.

In Chapter 6, I conclude this thesis and assess the possible future work on the mass function theory.

Reproduced with permission of the copyright owner. Further reproduction prohibited without permission.

Chapter 2

The Press-Schechter Theory

2.1 Introduction

In cosmological studies of the large scale structure of the universe, the mass distribution function plays an important discriminatory role. If we find the mass distribution function, then in principle we can distinguish between different candidate theories for structure formation. Especially the mass function is a crucial key to the nature of primordial density fluctuations from which the cosmic nonlinear structures are believed to have arisen through gravitational growth, recollapse, and virialization (Kolb & Turner 1990). Since these gravitational processes are inherently nonlinear and sufficiently complicated, it is not an easy task to find the mass distribution function for bound objects analytically. Owing to its important role in cosmology, however, much effort has been made on determining even an approximate expression of the mass function (e.g., Peebles 1985; Williams et al. 1991; Brainerd & Villumsen 1992; Cavaliere & Menci 1994; Vergassola et al. 1994; Cavaliere, Menci, & Tozzi 1996).

The pioneering attempt in this field has been ascribed to Press & Schechter (1974, hereafter PS) [1] who proposed an analytic formalism for the mass function

[1] See also Doroshkevich (1967).

Reproduced with permission of the copyright owner. Further reproduction prohibited without permission.

based on two simple assumptions: 1) the initial density field is Gaussian; 2) the gravitational collapse of mass elements is spherical and homogeneous. Along with these two assumptions, PS also postulated that the number densities of bound objects could be counted by filtering the initial linear density field. Although much criticism thereafter was poured upon the PS formalism about its unrealistic treatment of the collapse process and unclarified arguments including the *notorious* normalization factor of 2, the PS mass function has survived many numerical tests, showing good agreement with the results from N-body simulations (e.g., Efstathiou et al. 1988; Bond et al. 1991; Lacey & Cole 1994).

Motivated by somewhat unexpected success of the PS mass function, many authors have tried to understand why it works so well in practice. Especially, the controversial *fudge* normalization factor of 2 in the PS theory has been shown to be correct with a particular choice of a filter. Peacock & Heaven (1990) and Bond et al. (1991) have shown, by using the excursion set theory, that the fudge factor of 2 in the PS formalism which is directly related to the *cloud-in-cloud* problem can be justified with a sharp k-space filter. Jedamzik (1995) solved this cloud-in-cloud problem by means of the integral equation for the mass function. He insisted that the PS mass function should be altered even in the case of a sharp k-space filter. Yet Yano, Nagashima, & Gouda (1996) have found that the sharp k-space filter recovers the PS mass function with the normalization factor of 2 even in the Jedamzik formalism if a mathematically consistent definition of isolated bound objects is used and the spatial correlations are neglected.

In fact, most of the mass function theories developed afterwards have used the original PS idea as their foundations (Bond et al. 1991; Monaco 1995; Mo & White 1996; Audit et al. 1997; Lee & Shandarin 1998a). In this Chapter, we review this classical PS mass function theory. In § 2.2, we study the top-hat spherical model which provides an underlying dynamics to the PS formalism. In § 2.3, the statistical formalism of the original PS theory is described. In § 2.4, the

Reproduced with permission of the copyright owner. Further reproduction prohibited without permission.

normalization problem of the PS formalism and two different methods to solve this problem are explained. In § 2.5, we have a general discussion on the PS mass function theory.

2.2 The Top-Hat Spherical Model

The linear perturbation theory introduced in § 1.3 gives us an excellent approximation to how the initial density fluctuations evolve in the linear regime where $\delta \ll 1$. But the cosmic structures obviously correspond to $\delta \gg 1$, which implies that we have to somehow deal with the nonlinear regime in order to understand fully the formation of structures.

Unfortunately the complicated nature of the gravitational clustering process of the nonlinear regime resists all analysis. No single theory so far was able to describe satisfactorily the dynamics of the highly nonlinear regime (Sahni & Coles 1995). The only way to compromise is to simplify the real physics.

The top-hat spherical model provides us the *simplest* approximation to the nonlinear dynamics (Peebles 1980). The fundamental assumption which this model makes is that the gravitational collapse is spherical and homogeneous. Let us consider a spherically symmetric overdense region of radius R with an initial average overdensity contrast δ_i. In the case that the rest of the universe is flat, we can regard such a spherically overdense region as a mini-universe with $\Omega > 1$ included in a flat background universe. In other words, it is an island *closed* universe whose fate we can predict theoretically as explained in § 1.2.

As the background universe expands, it will expand together with the rest of the universe but at a progressively slower rate, so at some moment it will stop expanding, turn around, begin to collapse under its own gravitational force, and eventually form a bound object. On account of the spherical symmetry, the dynamics of the collapse process of the overdense regions is determined solely by the gravitational force due to the interior mass regardless of the mass of the

Reproduced with permission of the copyright owner. Further reproduction prohibited without permission.

background universe.

Let us study the above gravitational collapse process of the top-hat spherical model in mathematical detail. Starting with the energy conservation law, one can say

$$E = \frac{1}{2}\dot{R}^2(t) - \frac{GM}{R(t)} = \text{constant}. \tag{2.1}$$

Here M is the mass contained inside the given overdense region such that

$$M = \frac{4\pi}{3}R^3\bar{\rho}(1+\delta_i), \tag{2.2}$$

where $\bar{\rho}$ is the mean mass density of the background universe. As long as the dissipative force is negligible, we can assume that M is conserved during the whole gravitational collapse process.

At the initial time $t = t_i$, we can neglect that the peculiar velocities since δ is so small at t_i that the spherical overdense region may just expand along with the rest of the universe. Thus, we have

$$\dot{R}(t_i) = \left(\frac{\dot{a}}{a}\right)R(t_i) = H(t_i)R(t_i) \equiv H_iR_i, \tag{2.3}$$

where $H(t)$ is the Hubble parameter. So the kinetic energy is written as

$$K_i \equiv \left[\frac{\dot{R}(t_i)}{2}\right]^2 = \frac{H_i^2R_i^2}{2}. \tag{2.4}$$

Now one can express the potential energy at t_i in terms of K_i through equations (2.1)-(2.3):

$$\begin{aligned} U_i &= -\frac{GM}{R_i} = -\frac{4\pi}{3}G\bar{\rho}(t_i)R_i^2(1+\delta_i) \\ &= -\frac{1}{2}H_i^2R_i^2(1+\delta_i) = -K_i(1+\delta_i), \end{aligned} \tag{2.5}$$

since $\bar{\rho}(t_i) = \rho_c = 3H_i^2/8\pi G$ for the flat background universe [see §1.2.2]. Hence

Reproduced with permission of the copyright owner. Further reproduction prohibited without permission.

the total energy at t_i is written as

$$E = K_i + U_i = K_i - K_i(1 + \delta_i) = -K_i\delta_i. \tag{2.6}$$

Let us now find E at the instant of turning around, i.e., at $\dot{R}(t = t_{ta}) = 0$:

$$E = -\frac{GM}{R(t_{ta})} = -\frac{R(t_i)}{R(t_{ta})}K_i(1 + \delta_i), \tag{2.7}$$

since $GM = R_iK_i(1 + \delta_i)$ by equation (2.5). Through equations (2.6) and (2.7), we can relate $R(t_i) \equiv R_i$ to $R(t_{ta}) \equiv R_{ta}$ by:

$$\frac{R_t}{R_i} = \frac{1 + \delta_i}{\delta_i}. \tag{2.8}$$

Integrating equation (2.1) gives

$$R(\theta) = A(1 - \cos\theta), \qquad t(\theta) = B(\theta - \sin\theta), \tag{2.9}$$

with the integration constants A and B such that $A^3 = GMB^2$. At the turn-around moment of $\dot{R}(\theta) = 0$ which corresponds to $\theta = \pi$ by equation (2.9), the integration constants become

$$A = \frac{R_{ta}}{2}, \qquad B = \frac{t_{ta}}{2}. \tag{2.10}$$

Using equations (2.8)-(2.10), we finally have an equation describing the time evolution of $R(t)$ in terms of the initial conditions δ_i, R_i and H_i:

$$R(\theta) = \frac{R_i}{2}\left(\frac{1 + \delta_i}{\delta_i}\right)(1 - \cos\theta), \tag{2.11}$$

$$t(\theta) = \frac{1}{2H_i}\left(\frac{1 + \delta_i}{\delta_i^{\frac{3}{2}}}\right)(\theta - \sin\theta). \tag{2.12}$$

Expecting $\delta_i \ll 1$ and using $H_i = 2/3t_i$ according equation (1.7), we can also

Reproduced with permission of the copyright owner. Further reproduction prohibited without permission.

approximate the above equations such that

$$R(\theta) \approx \frac{R_i}{2\delta_i}(1-\cos\theta), \tag{2.13}$$

$$t(\theta) \approx \frac{3}{4}t_i\delta_i^{-\frac{3}{2}}(\theta-\sin\theta). \tag{2.14}$$

The time evolution of the density $\delta[\theta(t)]$ can be calculated straightforwardly with equations (2.2) and (2.11):

$$\delta[\theta(t)] = \frac{3M}{4\pi R^3(t)\bar{\rho}(t)} - 1 = \frac{9(\theta-\sin\theta)^2}{2(1-\cos\theta)^3} - 1. \tag{2.15}$$

In the linear limit of $\theta \ll 1$, equation (2.15) becomes

$$\delta \approx \frac{3\theta^2}{20} \approx \frac{3}{20}\left(\frac{6t}{B}\right)^{2/3}. \tag{2.16}$$

which agrees with the growing mode of the solution (1.14) obtained using the linear perturbation theory.

For comparison, let us consider the corresponding linearly extrapolated density contrast, δ_L. Through equations (2.15), (2.16) and (2.10), we have

$$\delta_L(\theta) = \frac{3}{5}\left(\frac{3}{4}\right)^{\frac{2}{3}}(\theta-\sin\theta)^{\frac{2}{3}}. \tag{2.17}$$

At the moment of recollapse when δ becomes infinity corresponding to $\theta = 2\pi$, equation (2.17) says

$$\delta_L(2\pi) = \frac{3}{5}\left(\frac{3}{4}\right)^{\frac{2}{3}}(2\pi)^{\frac{2}{3}} \approx 1.69. \tag{2.18}$$

Figure 2.1 plots the overdensity δ as a function of δ_L. Equation (2.18) and Figure 2.1 show that the spherical overdense region form a bound object when it's corresponding linearly extrapolated density contrast reaches ~ 1.69.

Reproduced with permission of the copyright owner. Further reproduction prohibited without permission.

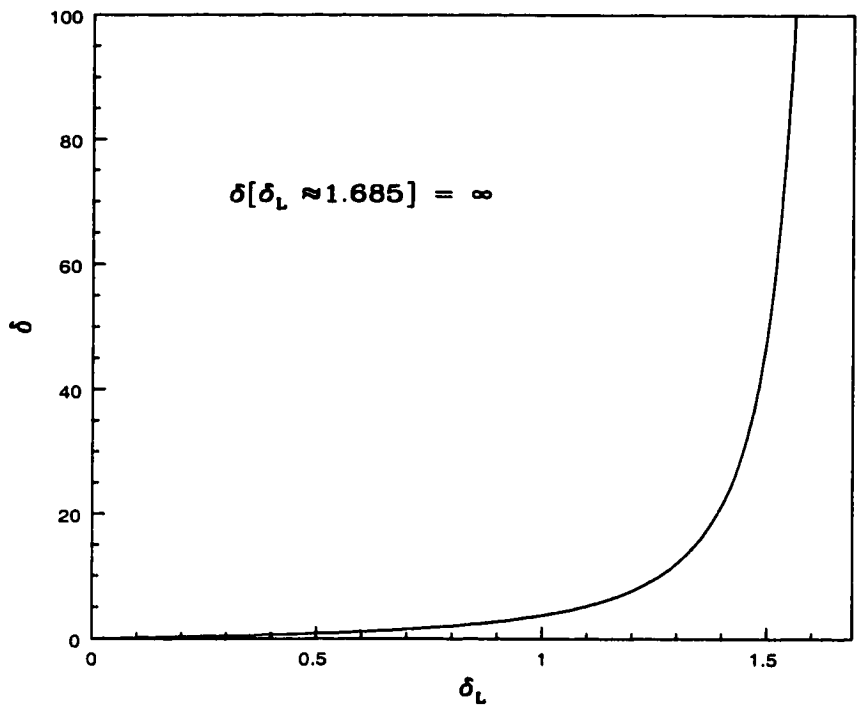

Figure 2.1: The real density contrast versus its linear extrapolated density contrast

2.3 Formalism

The mass function $n(M)$ is defined such that $n(M)dM$ is the comoving number density of gravitationally bound objects in the mass range $(M, M + dM)$. To compute this statistics, one first has to determine under what conditions the bound objects are formed. According to the top-hat spherical model described in § 2.2, the condition of a given region to collapse into a bound object is solely determined by the density of the region. But it is cumbersome to use the real density field directly since it is highly nonlinear at the stage of structure formation. Figure (2.1) shows that there is a one-to-one correspondence between the real density and the linearly extrapolated density in the top-hat spherical model. Besides, in the standard cosmology, the linear density field δ_L is assumed to be a Gaussian random field whose statistical properties are well known (Adler 1981). Thus it is convenient to use the corresponding linearly extrapolated density contrast of a

Reproduced with permission of the copyright owner. Further reproduction prohibited without permission.

region to determine whether it will form a bound object or not.

Let us consider a initial Gaussian density field $\delta(\mathbf{x})$ (δ without the subscript L is used to notate the linear density contrast from now on). The probability distribution of the Gaussian density field smoothed out by a filter function $W(R)$ of scale radius R is given by

$$p(\delta) = \frac{1}{\sqrt{2\pi}\sigma(M)} \exp\Big[-\frac{\delta^2}{2\sigma^2(M)}\Big], \tag{2.19}$$

where the mass variance $\sigma^2(M)$ is a function of scale mass $M \propto \bar{\rho}R^3$ depending on which filter to use. (see §1.3.2).

Now, let $F(M)$ be the fraction of the volumes occupied by the regions of the linear density field which will eventually collapse into bound objects. In the top-hat spherical model which the PS mass function theory is based on, the bound objects form in the regions where the linearly extrapolated density contrast δ, growing with time, reaches its critical value $\delta_c \simeq 1.69$ in a flat universe (see § 2.2 or Peebles 1993). Therefore the regions with $\delta > \delta_c$ when filtered at scale radius R correspond to the bound objects with masses greater than $M(R)$ since it will have $\delta = \delta_c$ when filtered at some larger scale. So the volume fraction $F(M)$ can be written as

$$F(M) = \frac{1}{\sqrt{2\pi}\sigma(M)} \int_{\delta_c}^{\infty} \exp\Big[-\frac{\delta^2}{2\sigma^2(M)}\Big] d\delta \tag{2.20}$$

$$= \frac{1}{2}\mathrm{erfc}\Big[\frac{\delta_c}{\sqrt{2}\sigma(M)}\Big], \tag{2.21}$$

where erfc(x) is the complementary error function.

The number densities of the bound objects with mass M, or, the mass function $n(M)$ can be obtained by differentiating $F(M)$ with respect to M, and then dividing dF/dM by the initial mean volume of bound objects, $M/\bar{\rho}$. But, before performing these algebra, let us note one obvious problem with the above analysis.

Reproduced with permission of the copyright owner. Further reproduction prohibited without permission.

The integral of dF/dM over the whole range of mass does not give unity:

$$\int_0^\infty \frac{dF}{dM} dM = \int_0^\infty dF = \frac{1}{2}. \tag{2.22}$$

PS avoided this normalization problem simply by multiplying dF/dM by a factor of 2, and wrote the mass function in the form such that

$$n_{ps}(M) = 2\frac{\bar{\rho}}{M}\left|\frac{dF}{dM}\right| = 2\frac{\bar{\rho}}{M}\left|\frac{d\sigma}{dM}\frac{\partial F}{\partial \sigma}\right| \tag{2.23}$$

$$= \sqrt{\frac{2}{\pi}}\frac{\bar{\rho}}{M}\left|\frac{d\sigma}{dM}\right|\frac{\delta_c}{\sigma^2(M)}\exp\left[-\frac{\delta_c^2}{2\sigma^2(M)}\right]. \tag{2.24}$$

Figure 2.2 plots the PS mass function for power law spectra $|\delta_k|^2 \propto k^n$. For every power index from $n = -2$ to $n = 1$, it is characterized by the exponential cut-off in the high mass section and the power-law slope in the low mass section.

Originally, PS argued that the mass from under dense regions would accrete on to bound objects in explaining their normalization factor of 2. But there is no point in their argument since the accretion of the mass from the under dense regions could cause at most a doubling of the mass of the bound objects not the number densities.

However, to PS luck, this normalization factor of 2 has turned out to be correct with a particular choice of filter. In the next section, we study the real physical meaning of the PS normalization factor of 2, and show how it can be justified.

2.4 The Cloud-in-Cloud Problem

As mentioned in § 2.1, the cooked-up normalization factor of 2 has been harshly criticized and regarded as the weakest point of the PS formalism. But for its practical success, the PS mass function would have been considered totally wrong and ignored completely.

In order to understand clearly where this normalization problem originated,

Reproduced with permission of the copyright owner. Further reproduction prohibited without permission.

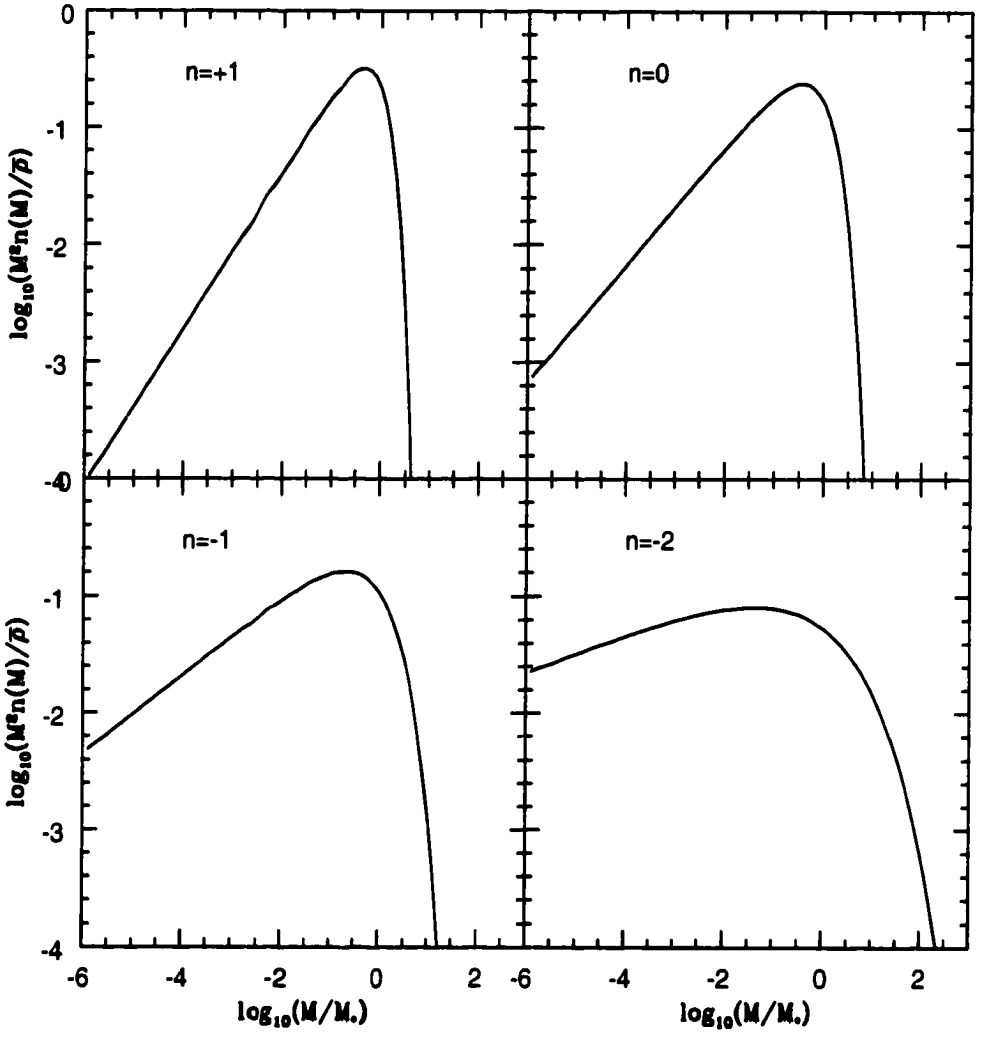

Figure 2.2: The PS mass function in logarithmic scale for power law spectra with $n = -2, -1, 0, 1$.

Reproduced with permission of the copyright owner. Further reproduction prohibited without permission.

let us consider the following arguments: Such regions with $\delta > \delta_c$ at a given filtering mass scale will have $\delta = \delta_c$ at some larger filtering mass scale. The PS formalism took care of those overdense regions ($\delta > \delta_c$) properly in calculating $F(M)$; Yet even for regions with $\delta < \delta_c$ at a given filtering scale, there is still a *nonzero* probability that such regions will have $\delta = \delta_c$ when filtered at some larger scale. But the PS formalism completely ignored those underdense regions in estimating $F(M)$. So half the mass initially present in the underdense regions was not accounted for. Those underdense regions embedded within overdense regions are called *cloud-in-clouds*, and the normalization factor of 2 is directly related to the amount of the occurrences of the cloud-in-clouds in the PS formalism.

Mysteriously, however, it turned out that the PS normalization factor of 2 is correct in the case of a sharp k-space filter (equation 1.18). There have been so far two different approaches to solve the normalization problem of the PS formalism. One is based on the *excursion set* theory, and the other is the Jedamzik formalism. In the following two subsections, we study these two different approaches to the cloud-in-cloud problem.

2.4.1 The Excursion-Set Approach

In this approach to the cloud-in-cloud problem, an additional term which takes care of the cloud-in-clouds is added to the equation (2.20) for the fraction of the volumes filled by the bound objects:

$$F(M) = F_0(M) + F_{cl}(M), \tag{2.25}$$

$$F_0(M) = \int_{\delta_c}^{\infty} p(\delta) d\delta. \tag{2.26}$$

Here $F_0(M)$ represents the fraction of the volumes occupied by the overdense regions with $\delta > \delta_c$ at a chosen filtering mass scale M, which is given by equation (2.21). And the additional term $F_{cl}(M)$ accounts for the amount of the cloud-

Reproduced with permission of the copyright owner. Further reproduction prohibited without permission.

in-clouds, i.e., the fractions of the volumes occupied by the underdense regions with $\delta < \delta_c$ at the scale M which will become "overdense" at some larger scale $M' > M$.

In order to calculate $F_{cl}(M)$, let us first consider a *survival* probability that a given underdense region never becomes overdense at any filtering scale, say, $M_1 > M_2 > \cdots > M_n > M$. This survival probability P_s can be expressed as

$$P_s \equiv \int_{-\infty}^{\delta_c} d\delta_1 \cdots \int_{-\infty}^{\delta_c} d\delta_n p_J(\delta_1, \cdots, \delta_n). \tag{2.27}$$

Here $p_J(\delta_1, \cdots, \delta_n)$ is the joint probability density distribution that a given region of the density field has the values of $\delta_1, \cdots, \delta_n$ at the filtering scales $M_1, \cdots, M_n > M$ respectively. $F_{cl}(M)$ now can be obtained by

$$F_{cl}(M) = 1 - P_s. \tag{2.28}$$

Thus, once P_s is computed, then we can find $F_{cl}(M)$ from equation (2.27). Unfortunately, however, calculating P_s as one can see, is quite formidable since it involves a multiple integral of the joint distribution.

Peacock & Heaven (1990) and Bond et al. (1991) have introduced a concept of "random walk" to calculate P_s, employing the excursion set theory. According to their idea, the process that a chosen point of the density field has each value of $\delta_1, \cdots, \delta_n$ at filtering scale $M_1, \cdots, M_n$ respectively can be viewed as a random walk of a point through $\delta_1, \cdots, \delta_n$. They showed that in the case of a sharp k-space filter, each step of random walk is independent from one another (Adler 1981). Consequently the survival probability P_s in the continuum limit obeys the following *diffusion* equation:

$$\frac{\partial}{\partial \sigma^2}\left(\frac{\partial P_s}{\partial \delta}\right) = \frac{1}{2}\frac{\partial^2 P_s}{\partial \delta^2}. \tag{2.29}$$

Reproduced with permission of the copyright owner. Further reproduction prohibited without permission.

with a boundary condition of

$$\left.\frac{\partial P_s(\delta)}{\partial \delta}\right|_{\delta_c} = 0. \tag{2.30}$$

This boundary condition amounts to saying that there is a barrier at $\delta = \delta_c$ in the process of a random walk, which in turn defines the underdense regions ($\delta < \delta_c$). With a help of some algebra, one can easily find the solution to the above equation:

$$\frac{\partial P_s}{\partial \delta} = -\frac{1}{\sqrt{2\pi}\sigma}\exp\left[-\frac{(\delta-\delta_c)^2}{2\sigma^2}\right] \tag{2.31}$$

$$P_s = \frac{1}{2}\mathrm{erf}\left[\frac{\delta_c}{\sqrt{2}\sigma}\right]. \tag{2.32}$$

Thus through equation (2.25),(2.28) and (2.32), one finds that

$$F(M) = \mathrm{erfc}\left[\frac{\delta_c}{\sqrt{2}\sigma}\right], \tag{2.33}$$

which is exactly twice the volume fraction of the original PS formalism [see equation (2.2)]. Therefore, the excursion-set approach provides a solution to the cloud-in-cloud problem of the PS formalism, justifying the normalization factor of 2 with a choice of a sharp k-space filter.

2.4.2 The Jedamzik Approach

Jedamzik (1995) approached the cloud-in-cloud problem of the PS formalism with a different point of view. Rather than dealing with the cloud-in-clouds directly, he modified the PS formula into the the following integral equation:

$$\left|\frac{dF}{dM}\right| = \frac{d}{dM}\left|\int_0^\infty dM' n(M')\frac{M'}{\bar{\rho}}P(M,M')\right|. \tag{2.34}$$

Here $P(M, M')$ is the conditional probability of finding a bound region with $\delta > \delta_c$ at filtering mass scale M, provided that it is included in an isolated bound object

Reproduced with permission of the copyright owner. Further reproduction prohibited without permission.

with mass $M'(> M)$. The isolated bound objects at a given epoch are those which have just collapsed without being included in larger bound objects. Therefore in the PS formalism, the isolated bound objects correspond to the regions with $\delta = \delta_c$ at a given filtering mass scale. Note the difference between the excursion-set approach and the Jedamzik formalism in interpreting $F(M)$. In the excursion-set approach, $F(M)$ is interpreted as the fraction of the volumes occupied by the bound regions just as it is in the original PS formalism, and thus a new additional term accounting for the cloud-in-clouds has been added to the PS formula for $F(M)$ in order to keep this interpretation. While in the Jedamzik approach, $F(M)$ is not the volume fraction but just the the probability that a given region has $\delta > \delta_c$ at a filtering mass scale M. In other words, rather than sticking to the original PS interpretation of the probability $F(M)$ as the volume fraction, Jedamzik found a correct relation between $F(M) = \int_{\delta_c}^{\infty} p(\delta) d\delta$ and the number densities of the bound objects, $n(M)dM$. Unfortunately, however, in his original paper Jedamzik did not use a consistent mathematical definition for a isolated bound object. As a result, he drew a wrong conclusion that the normalization factor 2 of the PS mass function is incorrect even in the case of a sharp k-space filter. Yano et al. (1996) found his mistake, and recovered the factor of 2 with a sharp k-space filter as mentioned in § 2.1.

Now, to solve equation (2.34), one first has to find the conditional probability $P(M, M')$ of the PS formalism. Again for the case of a sharp k-space filter, the conditional probability $P(M, M')$ becomes

$$\begin{aligned} P(M, M') &= P(\delta > \delta_c | \delta' = \delta_c) = \frac{P(\delta > \delta_c, \delta' = \delta_c)}{P(\delta' = \delta_c)}, \\ &= \frac{1}{\sqrt{2\pi(\sigma^2 - \sigma'^2)}} \int_{\delta_c}^{\infty} \exp\left[- \frac{(\delta - \delta_c')^2}{2(\sigma^2 - \sigma'^2)} \right] d\delta \\ &= \frac{1}{2} \Theta(M' - M), \end{aligned} \tag{2.35}$$

where (δ, σ) and (δ', σ') are the sets of the density and the mass variance at

Reproduced with permission of the copyright owner. Further reproduction prohibited without permission.

the *same* point but at the two different filtering mass scale M and $M'(> M)$ respectively.

Finally equation (2.34) becomes

$$\left|\frac{dF}{dM}\right| = 0.5\int_0^\infty dM' n(M')\frac{M'}{\bar{\rho}}\delta_D(M' - M) = 0.5\frac{M}{\bar{\rho}}n(M), \qquad (2.36)$$

where δ_D stands for the Dirac delta function. More explicitly,

$$n(M) = 2\frac{\bar{\rho}}{M}\left|\frac{dF}{dM}\right|, \qquad (2.37)$$

which is exactly the same PS formula as equation (2.23) but with the normalization factor of 2 included automatically.

Hence, the Jedamzik integral equation does solve the normalization problem of the PS formalism and justify the factor of 2 with a sharp k-space filter, too. But one merit of the Jedamzik approach over the one based on the excursion set theory is that the Jedamzik integral equation directly recovers the PS formula for the mass function without concerning about the occurrences of the cloud-in-clouds.

2.5 Discussion

The simplicity and the practical success of the PS mass function has resulted in its wide application. Cole & Kaiser (1988) used it to investigate the influence of galaxy clusters on CMBR through the Sunyaev-Zeldovich effect (Babbosa et al. 1996, Eke et al. 1996). Narayan & White (1998) predicted the gravitational lensing effect by dark halos with the PS mass function.

It has been also applied to study the galaxy formation at different redshifts (Cole & Kaiser 1989; White & Frenk 1991; Kauffmann, White, & Guiderdoni 1993), and the temperature distribution of X-ray clusters (Oukbir & Blanchard 1992; Viana & Liddle 1996).

Reproduced with permission of the copyright owner. Further reproduction prohibited without permission.

Bower (1991) and Bond et al. (1991) extended the PS mass function to relate the number densities of dark halos at two different epoch. Lacey & Cole (1993, 1994) used the extended PS mass function to calculate the halo merger rates. Yano et al. (1996) introduced two point correlation function into the PS mass function and analyzed the possible overlap effect between the collapsed objects. Fan et al. (1998) have investigated the evolution rate of structure formation using the PS mass function to determine the range of Ω. Lee & Shandarin (1998) use the PS formalism to study the biasing effect of the primordial gravitational potential on the formation of galaxy clusters. Indeed, it is generally believed that the PS formalism provides a useful statistical tool in analytical cosmology.

Nevertheless, it still leaves much to be desired. First, the gravitational collapse process should be treated in a more realistic model than the top-hat spherical one. Second, recent N-body simulations have detected that the numerical mass function is slightly flatter than the PS one especially in the high-mass section (e.g., Tormen 1998). That is, compared with the numerical mass functions the standard PS mass function underpredicts the number densities of high-mass objects but overpredicts at the characteristic mass scale. Third, N-body simulations also found a poor correlation between the location of bound objects and the peaks of the linear density field (Katz, Quinn, & Gelb 1993) although the PS formalism assumed that the bound objects form in the peaks of the density field. Fourth, the physical meaning of the sharp k-space filter which is the only filter to guarantee the proper normalization of the PS mass function has yet to be fully understood.

Reproduced with permission of the copyright owner. Further reproduction prohibited without permission.

Chapter 3

The Cosmological Mass Function in the Zel'dovich Approximation

3.1 Introduction

Since PS derived their mass function on the basis of the top-hat spherical model in 1974, the nonspherical nature of the gravitational collapse has been demonstrated by many authors (e.g., Shandarin et al. 1995; Kuhlman, Melott, & Shandarin 1996). Especially the shear has been shown to play a very important role in the formation of the nonlinear structures (e.g., Peebles 1990; Van de Weygaert & Babul 1994; Audit & Alimi 1996). Therefore it is necessary to consider more realistic dynamical models to understand the collapse process and find the mass function.

Monaco (1995) has suggested that the mass function should be treated as a Lagrangian quantity. Employing the Zel'dovich approximation as a proper Lagrangian dynamics, he computed the collapse epoch along the first principal axis, and showed that the shear shortens the collapse time and thus more high-mass structures are expected to form than the original PS mass function predicts. This effect of the shear can explain dynamically the lowered density threshold ($\delta_c \simeq 1.5$)

Reproduced with permission of the copyright owner. Further reproduction prohibited without permission.

detected in several N-body experiments (e.g., Efstathiou & Rees 1988; Carlberg & Couchman 1989; Klypin et al. 1995; Bond & Myers 1996).

Shandarin & Klypin (1984) have shown by N-body simulations that nonlinear clumps form from the Lagrangian regions where the smallest eigenvalue of the deformation tensor, λ_3, reaches a local maximum. Recently, Audit, Teyssier, & Alimi (1997) have proposed some analytic prescriptions to compute the collapse time along the second and the third principal axes, pointing out that Lagrangian dynamics is not valid after the first axis collapse but the formation of real virialized clumps must correspond to the third axis collapse. Their argument agrees with the N-body results obtained by Shandarin & Klypin (1984). In their analysis, the shear delays the third axis collapse rather than fastens it in contrast to its effect on the first axis collapse, which is in agreement with Peebles (1990).

The normalization problem, however, has not been well addressed in these nonspherical approaches to the mass function. In fact the nonspherical approach to the mass function helplessly encounters more complicated patterns of the cloud-in-cloud occurrences. Monaco (1995) adopted the normalization factor of 2 used in the PS formalism, arguing that in the high mass section the gravitational collapse is quasi spherical. While Audit et al. (1997) just assumed that the mass function could be normalized properly in any case.

At the core of the PS formalism based on the top-hat spherical model is the assumption that the condition for a given region to collapse into a bound object is purely determined by its local average density. And this simple assumption is represented by equation (2.20). Let us generalize equation (2.20) into the following one:

$$F(M) = \int_{-1}^{\infty} p(\delta) \cdot C d\delta, \tag{3.1}$$

where C stands for the probability that a given region with density will actually collapse. The specific functional form of C is determined by a chosen dynamics to describe the gravitational collapse process. Comparison of equation (3.1) with

Reproduced with permission of the copyright owner. Further reproduction prohibited without permission.

equation (2.20) reveals that in the PS formalism based on the top-hat spherical model, the collapse probability is nothing but the following Heavy-side step function.

$$C_{ps} = \Theta(\delta - \delta_c). \tag{3.2}$$

However, one can expect that in more realistic dynamical model than the simple top-hat spherical one, C must be given in more complex function than the above step one. Once $p(\delta)$ and C are determined, and then $F(M)$ is found, the mass function $n(M)$ can be easily obtained as

$$n(M) = \frac{\bar{\rho}}{M}\left|\frac{dF}{dM}\right|. \tag{3.3}$$

In this Chapter we study the eventual formation of clumps using a nonspherical dynamical model with fragmentation and coagulation effects ignored. We choose the Zel'dovich approximation as a suitable Lagrangian dynamics to take into account the nonspherical aspect of the gravitational collapse. However, instead of bringing the effect of the shear up to the surface, we try to retain the framework of the PS formalism, counting the number densities of bound objects from the filtered linear density field but with a different dynamical collapse probability C in equation (3.1). In § 3.2, the Zel'dovich approximation and its dynamical implications for the formation of clumps are described. § 3.3, two useful conditional probability distributions relating the density field to the collapse condition are derived, and a nonspherical collapse probability C is determined. In § 3.4 an *ansatz* is proposed to extend the validity of the Lagrangian dynamics to the third axis collapse. With a help of this ansatz a new analytic mass function for clumps is derived. In § 3.5 we justify the normalization factor 12.5 of the resulting mass function by using the Jedamzik integral equation. In § 3.6 the results are discussed and final conclusions are drawn. We relegate the detailed calculations and derivations to two Appendices.

Reproduced with permission of the copyright owner. Further reproduction prohibited without permission.

3.2 The Zel'dovich Approximation

The Zel'dovich approximation (Zel'dovich 1970) asserts that the trajectory of a cosmic particle in the comoving coordinates can be expressed by the following simple formula:

$$\mathbf{x} = \mathbf{q} - D_+(t)\nabla\Psi(\mathbf{q}). \tag{3.4}$$

Here $\mathbf{q}$ and $\mathbf{x}$ are the Lagrangian (initial) and the Eulerian (final) coordinates of the particle respectively, $D_+(t)$ describes the growth of density fluctuations as a function of time (see § 1.3.1), and $\Psi(\mathbf{q})$is the perturbation potential (initial velocity potential) which is a Gaussian random field related to the gravitational potential φ by $\varphi(\mathbf{q}) = 3H^2a^3\Psi(\mathbf{q})/2$.

Applying a simple mass conservation relation $\bar{\rho}d^3\mathbf{q} = \rho(\mathbf{x})d^3\mathbf{x}$ to the above formula (3.4) gives the following expression of the mass density:

$$\begin{aligned}\rho(\mathbf{x}) &= \bar{\rho}J\left[\frac{\partial^3\mathbf{q}}{\partial^3\mathbf{x}}\right] = \bar{\rho}\left|\delta_{ij} - D_+(t)d_{ij}\right| \\ &= \frac{\bar{\rho}}{[1 - D_+(t)\lambda_1(\mathbf{q})][1 - D_+(t)\lambda_2(\mathbf{q})][1 - D_+(t)\lambda_3(\mathbf{q})]},\end{aligned} \tag{3.5}$$

where J is the Jacobian of the transformation from the Lagrangian space to the Eulerian one, and λ_1, λ_2, λ_3 are the ordered eigenvalues ($\lambda_1 > \lambda_2 > \lambda_3$) of the deformation tensor d_{ij} defined by

$$d_{ij} \equiv \frac{\partial^2\Psi}{\partial q_i \partial q_j}. \tag{3.6}$$

Equation (3.5) shows that three random fields $\lambda_1(\mathbf{q})$, $\lambda_2(\mathbf{q})$, $\lambda_3(\mathbf{q})$ in the Lagrangian space are now new dynamic quantities determining the collapse condition of given cosmic masses in the corresponding Eulerian space. Thus the mass function of bound objects can be built upon this Lagrangian dynamical theory.

The usefulness of the Zel'dovich approximation in the single stream regime ($\sigma \geq 1$) where one-to-one correspondence between the Eulerian and the La-

Reproduced with permission of the copyright owner. Further reproduction prohibited without permission.

grangian spaces holds has been well demonstrated by many N-body simulations (e.g., Efstathious & Silk 1983). Although the Zel'dovich approximation fails like the other nonspherical dynamical models in the highly nonlinear regime or multi-stream regime where the one-to-one correspondence between the Eulerian and the Lagrangian space breaks down, it is in a dynamical sense true that the Zel'dovich approximation gives a most suitable guide to describe nonspherical gravitational collapse process in the single stream regime to which any PS-like formalism for the mass function must be restricted (Monaco 1995).

The actual dynamics for the formation of gravitationally bound objects is very complex. Even in the frame of the Zel'dovich approximation which is a first order Lagranigan dynamics, the description of the gravitational collapse along all three directions is far from being simple and too cumbersome to use (Arnol'd, Shandarin, & Zel'dovich 1982). Here we employ rather a simplified dynamical model purely based on equation (3.5) to approximate the collapse process and determine the collapse condition for the formation of clumps.

Provided that at least one of the eigenvalues is positive at a given (Lagrangian) point, the denominator in equation (3.5) can become zero as $D_+(t)$ increases with time, so the density $\rho(\mathbf{x})$ will diverge, signaling collapse at the corresponding Eulerian point. If only the largest eigenvalue is positive ($\lambda_1 > 0, \lambda_3 < \lambda_2 < 0$) in a given region, then it collapses along the first principal axis, forming a first nonlinear sheet-like structure - a pancake. If two eigenvalues are positive ($\lambda_1 > \lambda_2 > 0$) while the third one is negative ($\lambda_3 < 0$), then a two- dimensional structure - a filament forms, corresponding to the second axis collapse. The formation of a virialized bound object – a clump occurs only if all of three eigenvalues are positive, i.e. $\lambda_3 > 0$. So, in our dynamical model based on the Zel'dovich approximation, it is assumed that the lowest eigenvalue, λ_3, plays the most crucial role in determining the collapse condition for the formation of clumps. This assumption is in general agreement with the N-body simulations by Shandarin &

Reproduced with permission of the copyright owner. Further reproduction prohibited without permission.

Klypin (1984).

The useful joint probability distribution of an ordered set $(\lambda_1, \lambda_2, \lambda_3)$ is derived by Doroshkevich (1970):

$$p(\lambda_1, \lambda_2, \lambda_3) = \frac{3375}{8\sqrt{5}\pi\sigma^6} \exp\Big(- \frac{3I_1^2}{\sigma^2} + \frac{15I_2}{2\sigma^2}\Big)(\lambda_1 - \lambda_2)(\lambda_2 - \lambda_3)(\lambda_1 - \lambda_3), \quad (3.7)$$

where $I_1 = \lambda_1 + \lambda_2 + \lambda_3$, $I_2 = \lambda_1\lambda_2 + \lambda_2\lambda_3 + \lambda_3\lambda_1$, and σ^2 is the mass variance as defined in equation (1.17). From equation (3.7), one can see that the Zel'dovich approximation excludes both exactly spherical ($\lambda_1 = \lambda_2 = \lambda_3$) and exactly cylindrical ($\lambda_1 = \lambda_2$, $\lambda_2 = \lambda_3$, $\lambda_3 = \lambda_1$) collapse. Both types of collapse have zero probability of occurring. However, the points with $\lambda_i = \lambda_j$ exist in generic fields on lines, that is on a set of measure zero in 3-dimension, while the points with $\lambda_1 = \lambda_2 = \lambda_3$ do not exist at all.

In order to obtain deeper qualitative understanding of the collapse in the Zel'dovich approximation, it may be also useful, in addition to this joint probability distribution (3.7), to have individual probability distribution of each eigenvalue [1] (see Appendix A):

$$\begin{aligned} p(\lambda_1) &= \frac{\sqrt{5}}{12\pi\sigma}\Big\{20\frac{\lambda_1}{\sigma}\exp\Big(-\frac{9\lambda_1^2}{2\sigma^2}\Big) - \sqrt{2\pi}\exp\Big(-\frac{5\lambda_1^2}{2\sigma^2}\Big)\mathrm{erf}\Big(\sqrt{2}\frac{\lambda_1}{\sigma}\Big) \\ &\quad \times\Big(1 - 20\frac{\lambda_1^2}{\sigma^2}\Big) - \sqrt{2\pi}\exp\Big(-\frac{5\lambda_1^2}{2\sigma^2}\Big)\Big(1 - 20\frac{\lambda_1^2}{\sigma^2}\Big) \\ &\quad +3\sqrt{3\pi}\exp\Big(-\frac{15\lambda_1^2}{4\sigma^2}\Big)\mathrm{erf}\Big(\frac{\sqrt{3}\lambda_1}{2\sigma}\Big) + 3\sqrt{3\pi}\exp\Big(-\frac{15\lambda_1^2}{4\sigma^2}\Big)\Big\}, \quad (3.8) \end{aligned}$$

$$p(\lambda_2) = \frac{\sqrt{15}}{2\sqrt{\pi}\sigma}\exp\Big(-\frac{15\lambda_2^2}{4\sigma^2}\Big), \quad (3.9)$$

$$p(\lambda_3) = -\frac{\sqrt{5}}{12\pi\sigma}\Big\{20\frac{\lambda_3}{\sigma}\exp\Big(-\frac{9\lambda_3^2}{2\sigma^2}\Big) + \sqrt{2\pi}\exp\Big(-\frac{5\lambda_3^2}{2\sigma^2}\Big)\mathrm{erfc}\Big(\sqrt{2}\frac{\lambda_3}{\sigma}\Big)$$

[1] Doroshkevich (1970) derived the probability distribution of λ_1. But we found out a typo in his result. Except for the typo, equation (3.8) agrees with his result.

Reproduced with permission of the copyright owner. Further reproduction prohibited without permission.

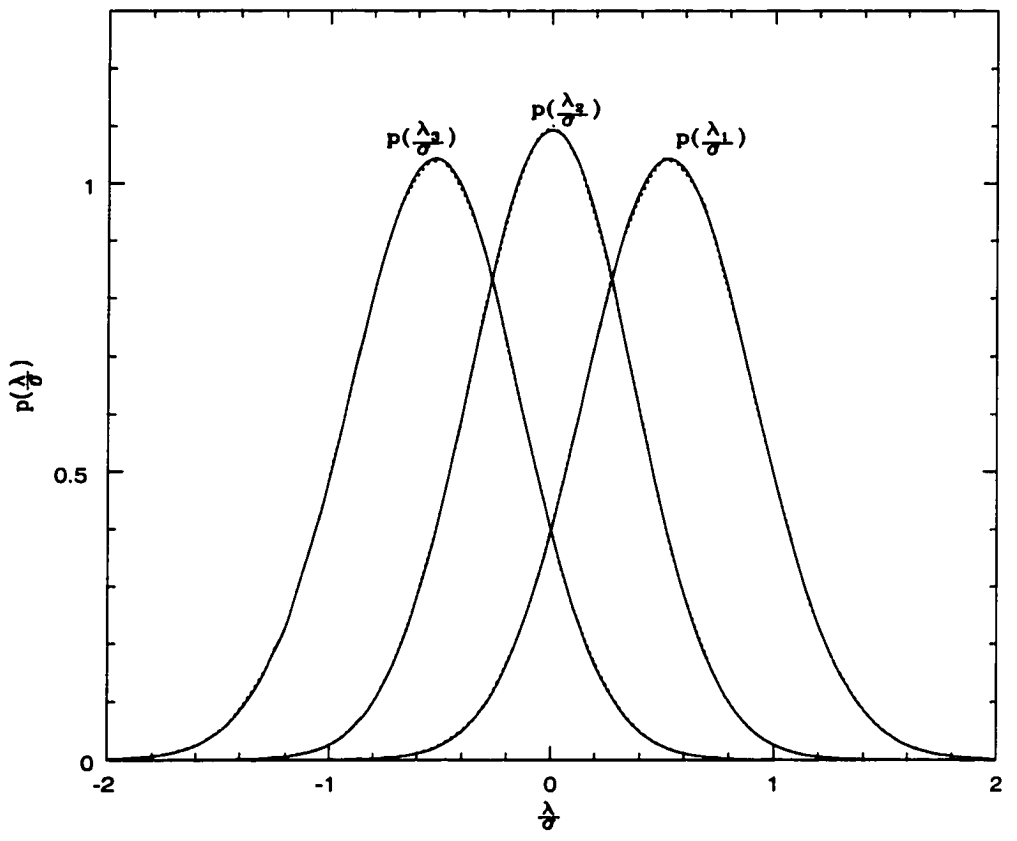

Figure 3.1: The individual probability distributions of three eigenvalues of the deformation tensor: The solid lines show the analytic results obtained in this paper for the rescaled variable λ/σ. The numerical results from the Monte Carlo simulation are also plotted as the dotted lines.

$$\times\Big(1-20\frac{\lambda_3^2}{\sigma^2}\Big)-3\sqrt{3\pi}\exp\Big(-\frac{15\lambda_3^2}{4\sigma^2}\Big)\mathrm{erfc}\Big(\frac{\sqrt{3}\lambda_3}{2\sigma}\Big)\Big\}. \tag{3.10}$$

The above individual probability distributions (3.8), (3.9), and (3.10) for the rescaled variable λ/σ are plotted in Figure 3.1. Note that the probability distribution of $\lambda_2(\mathbf{q})$ is Gaussian despite that $\lambda_2(\mathbf{q})$ is not a Gaussian random field.

According to equation (3.10), $\lambda_3 > 0$ has a low probability of occurring, 0.08 (see Doroshkevich 1970, or Appendix A). However, the small value of $P(\lambda_3 > 0) = 0.08$ does not indicate that only 8% of the whole regions will collapse into clumps.

Reproduced with permission of the copyright owner. Further reproduction prohibited without permission.

But rather it indicates that the probability of finding a bound region at filtering mass scale M is 0.08, provided that it is included in an isolated bound object with larger mass $M' > M$ (see § 3.5). Recall that the isolated bound objects indicate the bound objects at a given mass scale which have just collapsed at a given epoch but not included in yet larger bound objects (see § 2.4).

In the next section, we derive the conditional probabilities of $\lambda_3 > 0$ and δ, reveal the correlated properties between them, and determine a nonspherical collapse probability C.

3.3 Conditional Probabilities

In the linear regime when $D_+(t)$ is still less than unity, equation (3.5) can be approximated by

$$\rho \simeq \bar{\rho}[1 + D_+(\lambda_1 + \lambda_2 + \lambda_3)]. \tag{3.11}$$

Setting $D_+ \equiv 1$ at the present epoch, the linearly extrapolated density contrast is now written as

$$\delta = \frac{\delta\rho}{\bar{\rho}} = \lambda_1 + \lambda_2 + \lambda_3. \tag{3.12}$$

Let us choose $(\delta, \lambda_2, \lambda_3)$ as a new set of variables. Then equation (3.7) can be reexpressed as a joint probability distribution of $(\delta, \lambda_2, \lambda_3)$ such that

$$\begin{aligned} p(\delta, \lambda_2, \lambda_3) &= \frac{3375}{8\pi\sqrt{5}\sigma^6} \exp\left[-\frac{3\delta^2}{\sigma^2} + \frac{15}{2\sigma^2}(\lambda_2 + \lambda_3)(\delta - \lambda_2 - \lambda_3) + \frac{15}{2\sigma^2}\lambda_2\lambda_3 \right] \\ &\quad \times(\delta - 2\lambda_2 - \lambda_3)(\lambda_2 - \lambda_3)(\delta - \lambda_2 - 2\lambda_3). \end{aligned} \tag{3.13}$$

Direct integration of the above joint distribution (3.13) over λ_2 gives the two point probability distribution of (δ, λ_3):

$$p(\delta, \lambda_3) = \int_{\lambda_3}^{\frac{\delta-\lambda_3}{2}} p(\delta, \lambda_2, \lambda_3) d\lambda_2$$

Reproduced with permission of the copyright owner. Further reproduction prohibited without permission.

$$= \frac{3\sqrt{5}}{16\pi\sigma^4}\Big(15\delta^2 - 90\lambda_3\delta + 135\lambda_3^2 - 8\sigma^2\Big)\exp\Big(-\frac{9\delta^2 - 30\lambda_3\delta + 45\lambda_3^2}{8\sigma^2}\Big)$$
$$+\frac{3\sqrt{5}}{2\sigma^2\pi}\exp\Big(-\frac{6\delta^2 - 30\lambda_3\delta + 45\lambda_3^2}{2\sigma^2}\Big), \tag{3.14}$$

where the upper limit and the lower limit of λ_2 are $(\delta - \lambda_3)/2$ and λ_3 respectively due to the condition of $\lambda_1 > \lambda_2 > \lambda_3$. With equation (3.14), we can investigate various correlated properties between δ-field and λ_3-field.

First of all, let us calculate the probability distribution of δ confined in the regions with $\lambda_3 > 0$:

$$p(\delta|\lambda_3 > 0) = \frac{p(\delta, \lambda_3 > 0)}{P(\lambda_3 > 0)} = \frac{\int_0^{\frac{\delta}{3}} p(\delta, \lambda_3)d\lambda_3}{P(\lambda_3 > 0)}$$
$$= \Big\{-\frac{75\sqrt{5}}{8\pi\sigma^2}\delta\exp\Big(-\frac{9\delta^2}{8\sigma^2}\Big) + \frac{25}{4\sqrt{2\pi}\sigma}\exp\Big(-\frac{\delta^2}{2\sigma^2}\Big)$$
$$\times\Big[\mathrm{erf}\Big(\frac{\delta\sqrt{10}}{4\sigma}\Big) + \mathrm{erf}\Big(\frac{\delta\sqrt{10}}{2\sigma}\Big)\Big]\Big\}\Theta(\delta). \tag{3.15}$$

Here the condition $\lambda_1 > \lambda_2 > \lambda_3$ is used again to determine $\delta/3$ for the upper limit of λ_3. Figure 3.2 compares the unconditional Gaussian distribution of the density field (2.19) with this conditional probability distribution (3.15) for the rescaled variable δ/σ. It is shown that the maximum of $p(\delta|\lambda_3 > 0)$ is reached when $\delta \simeq 1.5\sigma$. That is, the linearly extrapolated density of the regions satisfying $\lambda_3 > 0$ is most likely to be around 1.5σ. The average density contrast, $< \delta >_{\lambda_3>0}$, can be also computed with equation (3.15):

$$< \delta >_{\lambda_3>0} = \int_0^\infty \delta p(\delta|\lambda_3 > 0)d\delta = \frac{25\sqrt{10}\sigma}{144\sqrt{\pi}}(3\sqrt{6} - 2) \simeq 1.65\sigma. \tag{3.16}$$

So in the regions with $\lambda_3 > 0$, the average density $< \delta >_{\lambda_3>0}$ is slightly higher than the most probable density, say $\delta^{max}_{\lambda_3>0}$. We note that for $\sigma = 1$, $\delta^{max}_{\lambda_3>0}$ roughly coincides with the lowered density threshold $\delta_c \simeq 1.5$ of the PS mass function, while $< \delta >_{\lambda_3>0}$ is close to the spherical threshold value $\delta_c \simeq 1.69$. Setting

Reproduced with permission of the copyright owner. Further reproduction prohibited without permission.

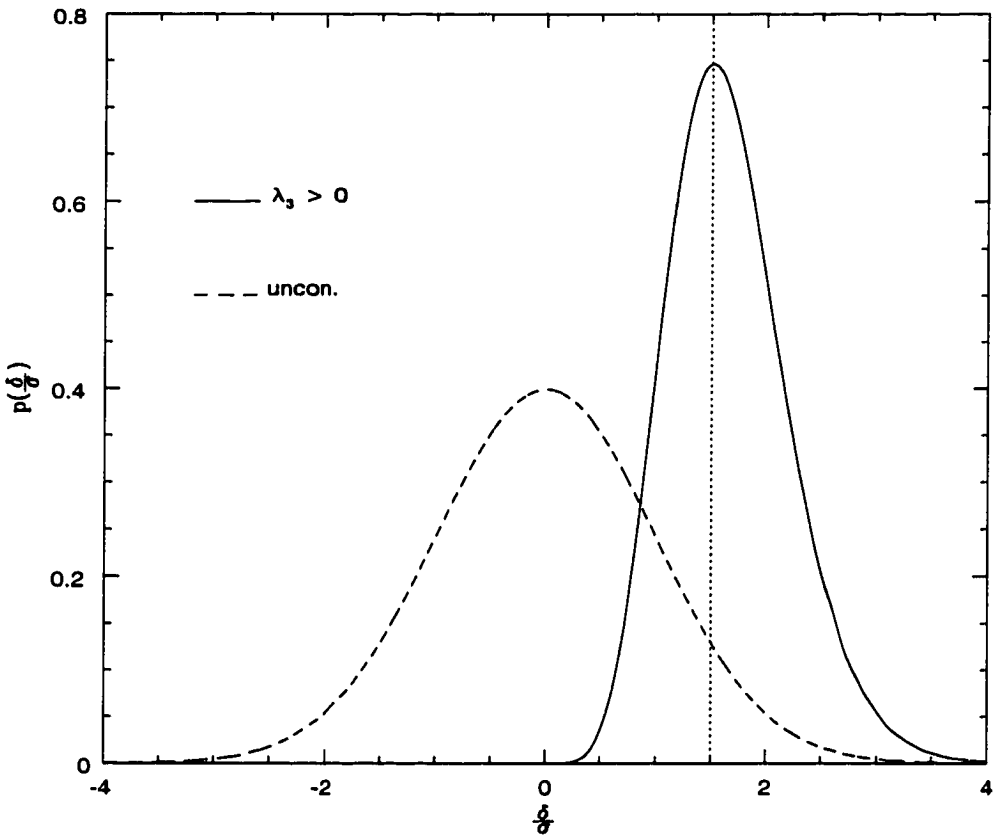

Figure 3.2: The probability distribution of the rescaled density field, (δ/σ). The solid line represents the rescaled density distribution under the condition of $\lambda_3 > 0$, while the dashed line shows the unconditional Gaussian distribution. The vertical dotted line indicates the position of $\delta/\sigma = 1.5$.

$\sigma = 1$ means filtering the density field on characteristic mass scale M_0 [defined by $\sigma(M_0) = 1$]. Thus the regions with $\lambda_3 > 0$ for $\sigma = 1$ correspond to clumps with masses $M > M_0$. As a matter of fact, as mentioned in § 3.1, it is unavoidable to limit our Lagrangian dynamical approach to the high-mass section $(M > M_0)$ since the Zel'dovich approximation is valid only in the single stream regions, while the multistream regions are rare for $M > M_0$ (Kofman et al. 1994).

Another conditional distribution worth deriving is $P(\lambda_3 > 0|\delta)$, the probability

Reproduced with permission of the copyright owner. Further reproduction prohibited without permission.

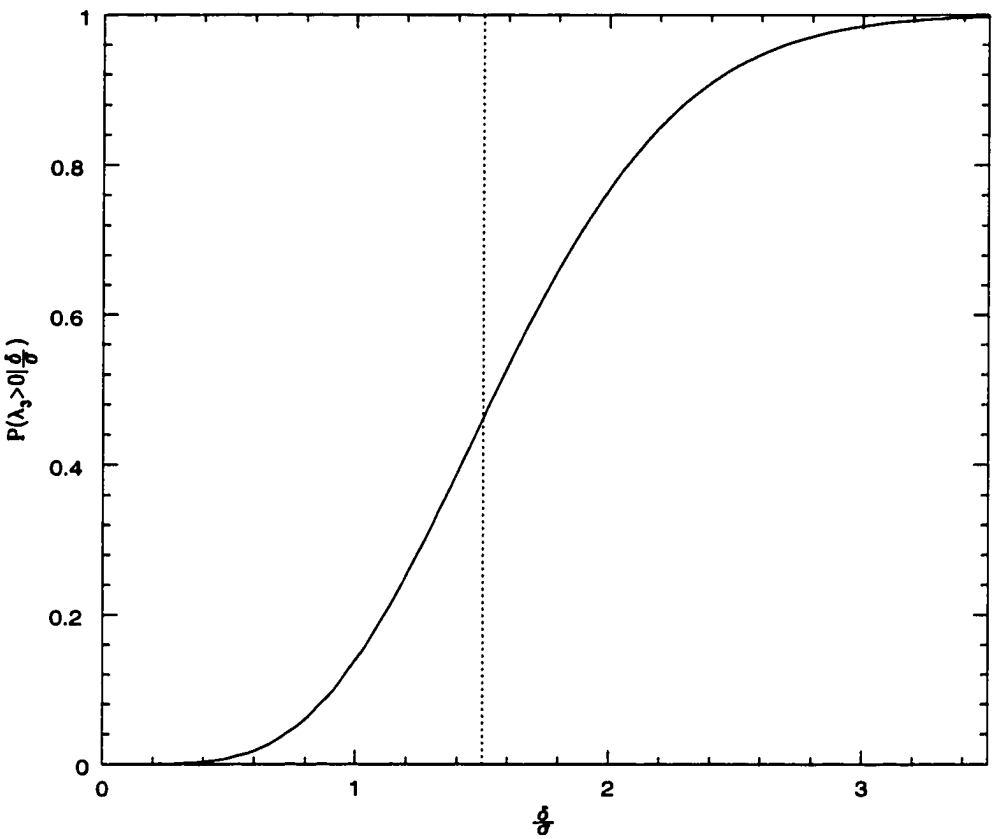

Figure 3.3: The conditional probability of $\lambda_3 > 0$ as a function of the rescaled density δ/σ. The vertical dotted line indicates the position $\delta/\sigma = 1.5$.

that a given region with density δ will have all positive eigenvalues:

$$\begin{aligned} P(\lambda_3 > 0|\delta) &= \frac{p(\delta, \lambda_3 > 0)}{p(\delta)} \\ &= \Big\{ -\frac{3\sqrt{10}}{4\sqrt{\pi}\sigma}\delta \exp\Big(-\frac{5\delta^2}{8\sigma^2}\Big) \\ &\qquad + \frac{1}{2}\Big[\mathrm{erf}\Big(\frac{\delta\sqrt{10}}{4\sigma}\Big) + \mathrm{erf}\Big(\frac{\delta\sqrt{10}}{2\sigma}\Big)\Big]\Big\}\Theta(\delta). \end{aligned} \tag{3.17}$$

The resulting conditional probability (3.16) for the rescaled variable δ/σ is plotted in Figure 3.3. The probability of $\lambda_3 > 0$ begins to exceed one-half when $\delta \simeq 1.5\sigma$, and reaches unity when $\delta \simeq 3\sigma$. This implies that the collapse of highly

Reproduced with permission of the copyright owner. Further reproduction prohibited without permission.

overdense regions ($\delta \gg \sigma$) will be always along all three directions (Bernardeau 1994). We take equation (3.17) as our nonspherical collapse probability C and proceed to derive the mass function of clumps analytically in the next section.

3.4 Derivation

As noted earlier, the Zel'dovich approximation as a first order Lagrangian theory works very well till the first orbit crossing (corresponding to the formation of pancakes) but breaks down afterwards in the multistream regime (Shandarin & Zel'dovich 1989). Therefore the rather restrictive collapse condition purely based on this Lagrangian formalism may not be fully satisfactory to describe the formation of clumps, especially low-mass objects.

On the other hand, Shandarin & Klypin (1984) have shown by N-body simulations that the clumps form from the Lagrangian regions where the smallest eigenvalue λ_3 of the deformation tensor reaches a local maximum. Thus, one practical way to overcome the limited validity of the Zel'dovich approximation within the framework of our dynamical approach to mass functions is to parameterize the collapse condition by $\lambda_3 > \lambda_{3c}$, assuming that the critical value of λ_{3c} is a free parameter. Employing this simple *ansatz* to derive $n(M)$, we first calculate the following probability distribution with equations (2.19) and (3.14)

$$\begin{aligned} P(\lambda_3 > \lambda_{3c}|\delta) &= \frac{p(\delta, \lambda_3 > \lambda_{3c})}{p(\delta)} = \frac{\int_{\lambda_{3c}}^{\frac{\delta}{3}} p(\delta, \lambda_3) d\lambda_3}{p(\delta)} \\ &= \left\{ -\frac{3\sqrt{10}}{4\sqrt{\pi}\sigma}(\delta - 3\lambda_{3c}) \exp\left[-\frac{5(\delta - 3\lambda_{3c})^2}{8\sigma^2} \right] \right. \\ &\quad \left. + \frac{1}{2}\left\{ \mathrm{erf}\left[\frac{(\delta - 3\lambda_{3c})\sqrt{10}}{4\sigma} \right] + \mathrm{erf}\left[\frac{(\delta - 3\lambda_{3c})\sqrt{10}}{2\sigma} \right] \right\} \right\} \\ &\quad \times \Theta(\delta - 3\lambda_{3c}). \end{aligned} \tag{3.18}$$

Comparison of equation (3.18) with equation (3.17) reveals that $P(\lambda_3 > \lambda_{3c}|\delta)$

Reproduced with permission of the copyright owner. Further reproduction prohibited without permission.

is just horizontally shifted along δ-axis by $3\lambda_{3c}$ from $P(\lambda_3 > 0|\delta)$ with its shape unchanged.

Consequently, this ansatz is mathematically equivalent to parallel transformation of the density field itself by $-3\lambda_{3c}$. Thus equation (3.1) is now expressed as follows:

$$\begin{aligned} F(M) &= \int_{-\infty}^{\infty} p(\delta + 3\lambda_{3c}) \cdot P(\lambda_3 > 0|\delta) d\delta \\ &= \frac{1}{\sqrt{2\pi}\sigma} \int_0^{\infty} \exp\Big[- \frac{(\delta + 3\lambda_{3c})^2}{2\sigma^2} \Big] \Big\{ - \frac{75\sqrt{10}}{8\sqrt{\pi}\sigma} \delta \exp\Big(- \frac{5\delta^2}{8\sigma^2} \Big) \\ &\quad + \frac{25}{4} \Big[\mathrm{erf}\Big(\frac{\delta\sqrt{10}}{4\sigma} \Big) + \mathrm{erf}\Big(\frac{\delta\sqrt{10}}{2\sigma} \Big) \Big] \Big\} d\delta. \end{aligned} \tag{3.19}$$

Here the volume fraction $F(M)$ is normalized by a factor of $1/0.08 = 12.5$ which we justify with a sharp k-space filter in § 5. However this larger normalization factor can be understood as in the followings (see § 3.5). In an ideal hierarchical model, all the masses are included in clumps. According to our dynamical model, only about 8% of all the masses are included in the clumps with the "largest" mass (the "largest mass" of bound objects in the universe is, in a practical sense, $M \simeq M_0$). This is in rough agreement with the fraction of the galaxies in the Abell clusters (e.g., Padmanabhan 1993). All the remaining masses are included in the clumps at smaller filtering mass scales.

Differentiating equation (3.18) with respect to σ, we have

$$\begin{aligned} \frac{\partial F}{\partial \sigma} &= \frac{\partial}{\partial \sigma} \Big\{ \frac{1}{\sqrt{2\pi}\sigma} \int_0^{\infty} \exp\Big(- \frac{(\delta + 3\lambda_{3c})^2}{2\sigma^2} \Big) \Big\{ - \frac{75\sqrt{10}}{8\sqrt{\pi}\sigma} \delta \exp\Big(- \frac{5\delta^2}{8\sigma^2} \Big) \\ &\qquad + \frac{25}{4} \Big[\mathrm{erf}\Big(\frac{\delta\sqrt{10}}{4\sigma} \Big) + \mathrm{erf}\Big(\frac{\delta\sqrt{10}}{2\sigma} \Big) \Big] \Big\} d\delta \Big\}, \\ &= \frac{25\sqrt{10}\lambda_{3c}}{2\sqrt{\pi}\sigma^2} \Big(\frac{5\lambda_{3c}^2}{3\sigma^2} - \frac{1}{12} \Big) \exp\Big(- \frac{5\lambda_{3c}^2}{2\sigma^2} \Big) \mathrm{erfc}\Big(\frac{\sqrt{2}\lambda_{3c}}{\sigma} \Big) \\ &\quad + \frac{25\sqrt{15}\lambda_{3c}}{8\sqrt{\pi}\sigma^2} \exp\Big(- \frac{15\lambda_{3c}^2}{4\sigma^2} \Big) \mathrm{erfc}\Big(\frac{\sqrt{3}\lambda_{3c}}{2\sigma} \Big) \end{aligned}$$

Reproduced with permission of the copyright owner. Further reproduction prohibited without permission.

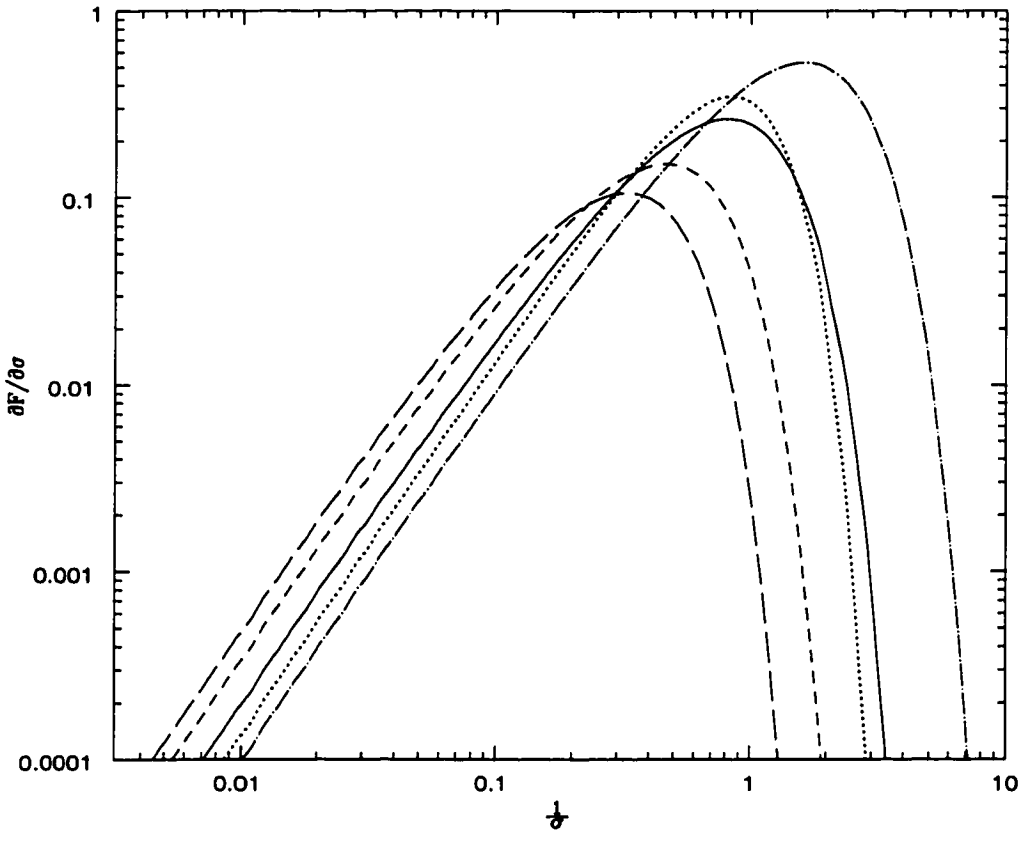

Figure 3.4: The differential volume fraction for $\lambda_{3c} = 0.1, 0.4, 0.7$ and 1.0 (dot-dashed, solid, dashed and long-dashed lines). The dotted line is the standard ($\delta_c \simeq 1.69$) PS differential volume fraction.

$$-\frac{125\sqrt{5}\lambda_{3c}^2}{6\pi\sigma^3}\exp\Big(-\frac{9\lambda_{3c}^2}{2\sigma^2}\Big). \tag{3.20}$$

Figure 3.4 shows the generic behavior of this differential volume fraction (3.20) as λ_{3c} changes. Since $\partial F/\partial\sigma$ is directly proportional to $n(M)$, one can conclude from Figure 3.4 that as λ_{3c} increases, the number densities of small-mass clumps (large σ) increase while the large masses (small σ) are reduced and the peak is lowered.

Reproduced with permission of the copyright owner. Further reproduction prohibited without permission.

For simple power law spectra $|\delta_k|^2 \propto k^n$, the mass variance becomes

$$\sigma^2(M) = \left(\frac{M}{M_0}\right)^{-(n+3)/3}. \tag{3.21}$$

So in this case, the mass function can be expressed explicitly in terms of M:

$$\begin{aligned} n(M) &= \frac{\bar{\rho}}{M}\left|\frac{dF}{dM}\right| = \frac{\bar{\rho}}{M}\left|\frac{d\sigma}{dM}\frac{\partial F}{\partial \sigma}\right| \\ &= \frac{25\sqrt{10}\lambda_{3c}}{2\sqrt{\pi}}\left(\frac{n+3}{6}\right)\frac{\bar{\rho}}{M^2}\left(\frac{M}{M_0}\right)^{(n+3)/6} \times \\ &\quad \left\{\left[\frac{5\lambda_{3c}^2}{3}\left(\frac{M}{M_0}\right)^{(n+3)/3} - \frac{1}{12}\right]\exp\left[-\frac{5\lambda_{3c}^2}{2}\left(\frac{M}{M_0}\right)^{(n+3)/3}\right]\right. \\ &\quad \times \mathrm{erfc}\left[\sqrt{2}\lambda_{3c}\left(\frac{M}{M_0}\right)^{(n+3)/6}\right] \\ &\quad + \frac{\sqrt{6}}{8}\exp\left[-\frac{15\lambda_{3c}^2}{4}\left(\frac{M}{M_0}\right)^{(n+3)/3}\right]\mathrm{erfc}\left[\frac{\sqrt{3}\lambda_{3c}}{2}\left(\frac{M}{M_0}\right)^{(n+3)/6}\right] \\ &\quad \left. - \frac{5\lambda_{3c}}{3\sqrt{2\pi}}\left(\frac{M}{M_0}\right)^{(n+3)/6}\exp\left[-\frac{9\lambda_{3c}^2}{2}\left(\frac{M}{M_0}\right)^{(n+3)/3}\right]\right\}. \end{aligned} \tag{3.22}$$

We display the resulting mass function for $\lambda_{3c} \approx 0.37$ in Figure 3.5. The value of 0.37 for λ_{3c} is chosen to make our results for the high-mass section fit well with the $\delta_c \approx 1.5$ PS mass function which is generally in good agreement with recent N-body results as mentioned in §3.1. The original PS mass function with $\delta_c \simeq 1.69$ is also shown for comparison. For every power index n from -2 to 1, the mass function (3.22) is characterized by the following properties:

(1) In the high-mass section ($M/M_0 > 1$), it fits quite well with the $\delta_c \simeq 1.5$ PS mass function.

(2) Its peak is lower than that of the PS one, which agrees with N-body results (e.g., see Efstathious et al. 1988).

(3) It has approximately the same slope as the PS mass function but predicts more structures in the low-mass section ($M/M_0 < 1$).

In short, our mass function with $\lambda_{3c} \approx 0.37$ is shown to be slightly *flatter* in

Reproduced with permission of the copyright owner. Further reproduction prohibited without permission.

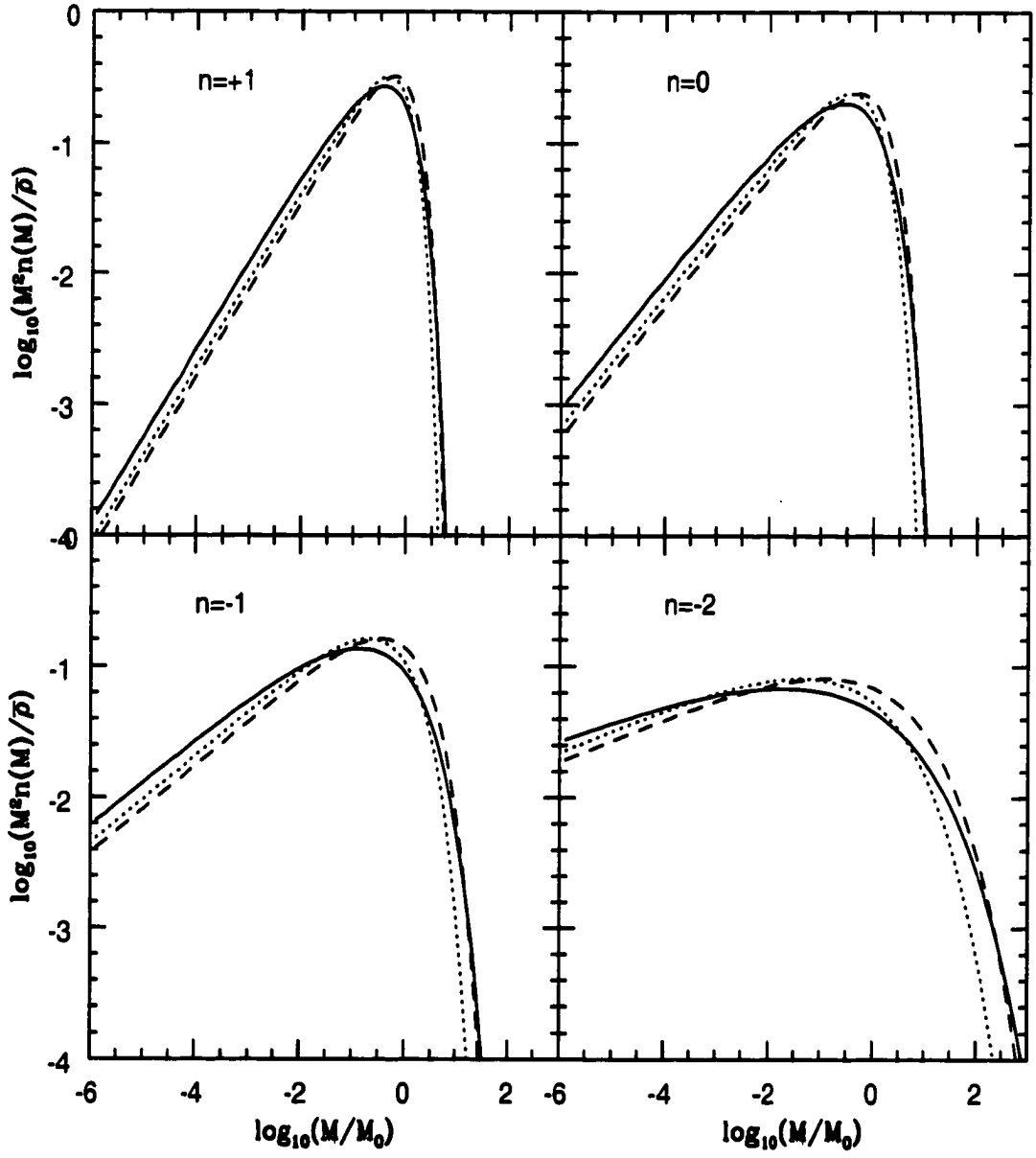

Figure 3.5: The mass function for the power index $n = +1, 0, -1$ and -2. The solid lines show our analytic results with $\lambda_{3c} = 0.37$, while the dashed and dotted lines represent the PS mass function with $\delta_c = 1.5$ and 1.69 respectively.

Reproduced with permission of the copyright owner. Further reproduction prohibited without permission.

shape but generally agrees well with the PS one.

3.5 Normalization

Up to now, following the PS-like approach, we assumed that equation (3.2) is correct. In other words, the probability of finding a region with $\lambda_3 > \lambda_{3c}$ at filtering mass scale M is assumed to be proportional to the fraction of the volume occupied by the regions which will eventually collapse into bound objects with masses $\geq M$.

Strictly speaking, however, the original PS formula (3.3) is not quite correct as mentioned in § 2.4 since the resulting mass function has to be always renormalized. Even in the regions with $\lambda_3 < \lambda_{3c}$ at the filtering mass scale M, there is still a nonzero probability of $\lambda_3 = \lambda_{3c}$ when the density field is filtered at some larger scale $M'(> M)$. But this marginal probability is ignored by the PS-like approach, which has resulted in a large normalization factor 12.5 of our mass function.

We employ the Jedamzik integral equation (2.34) to solve our normalization problem. In our formalism, the conditional probability $P(M, M')$ is the probability of finding a bound region ($\lambda_3 > \lambda_{3c}$) at filtering mass scale M, provided that it is included in an isolated bound object with mass $M'(> M)$. And the isolated bound objects are those which have just collapsed without being included yet in larger objects so correspond to the regions $\lambda_3 = \lambda_{3c}$ at a given filtering mass scale.

We find that the conditional probability $P(M, M')$ for the case of a sharp k-space filter can be approximated by (see Appendix B):

$$P(M, M') = 0.08\Theta(M' - M), \tag{3.23}$$

when M' is much larger than M. Equation (3.23) reveals that $P(\lambda_3 > 0) = 0.08$ results in $P(M, M') = 0.08$ $(M < M')$. So, in our formalism the probability of finding a bound region ($\lambda_3 > \lambda_{3c}$) of mass scale M included in an isolated bound

Reproduced with permission of the copyright owner. Further reproduction prohibited without permission.

region ($\lambda_3 = \lambda_{3c}$) with mass greater M is only 0.08. And this is directly related to our normalization factor of $1/0.08 = 12.5$, just as in the PS formalism the probability $P(M, M') = 0.5$ is directly related to the PS normalization factor of $1/0.5 = 2$.

Now, with equation (3.24) and (3.23), we have

$$\left|\frac{dF}{dM}\right| = 0.08 \int_0^\infty dM' n(M') \frac{M'}{\bar{\rho}} \delta_D(M' - M) = 0.08 \frac{M}{\bar{\rho}} n(M), \tag{3.24}$$

or, more evidently,

$$n(M) = 12.5 \frac{\bar{\rho}}{M} \left|\frac{dF}{dM}\right|, \tag{3.25}$$

which is exactly the same formula as equation (2.2) but with the normalization factor of 12.5 included explicitly.

Thus the Jedamzik integral equation also justifies the normalization factor 12.5 of our mass function in the case of a sharp k-space filter.

3.6 Discussion and Conclusions

We have derived a new *analytic* mass distribution function for clumps different from the PS one. The underlying dynamics has been described by the Zel'dovich approximation which treats the nonspherical gravitational collapse. Similar to Shandarin & Klypin (1984) and Audit et al. (1997), we have assumed that the clumps would be formed by the mass elements which have experienced gravitational collapse along all three directions.

We have given a somewhat different interpretation to the PS analysis by reexpressing the fraction of the volume occupied by the bound regions in terms of two probabilities: the probability of the Gaussian density distribution and the collapse probability of the given dense regions. The Zel'dovich approximation has led us to determine a nonspherical collapse probability which is different from the PS

Reproduced with permission of the copyright owner. Further reproduction prohibited without permission.

one, relating the density field to the positive lowest eigenvalue of the deformation tensor.

We have shown that the collapse probability reaches almost unity when $\delta > 3\sigma$, which indicates that the highly overdense regions will always collapse along all three directions. In addition, we have found the density distribution of the regions which meet the collapse condition based on the Zel'dovich approximation. This distribution has shown that the most probable density contrast of such regions is around 1.5 at the characteristic mass scale M_0.

We have proposed a simple *ansatz* in order to treat the multistream regions where the Lagrangian dynamics is not applicable. This ansatz has enabled us to derive an analytic mass function characterized by one free parameter, λ_{3c}. The best approximate value of this parameter has been chosen to be $\lambda_{3c} \simeq 0.37$. We admit that there is no background dynamical theory for determining directly the value of this free parameter which thus has to be found phenomenologically. However, the following arguments may give a hint to understand why this parameter has this value. A simple extrapolation of equation (3.5) into the multistream regions suggests that only the mass elements with $\lambda_3 > \lambda_{3c} = 1$ collapse along all three directions by the present epoch of $D_+ = 1$. However, the collapse along the first two directions increases the density, which therefore speeds up the collapse along the third directions. This roughly agrees with the conclusion of Audit et al. (1997). Using equation (24) from Audit et al. (1997) with their choice of the parameters ($\epsilon = 1, \alpha = 0.8, \delta_c = 1.69, \sigma_c = 0.74$), one can easily obtain for the collapse epoch $a_c = 1/(0.8\lambda_3 + 0.32\delta)$ that is always earlier than the prediction of the Zel'dovich approximation ($a_c = 1/\lambda_3$) provided that $\lambda_3 > 0$.

For power law spectra, it has been shown that our resulting mass function with $\lambda_{3c} \simeq 0.37$ is in good agreement with the $\delta_c \simeq 1.5$ PS mass function in the high-mass section, but has lower peak and predicts more small-mass structures, which are in agreement with what has been detected in N-body simulations (e.g.,

Reproduced with permission of the copyright owner. Further reproduction prohibited without permission.

Efstathious et al. 1988; Peacock & Heavens 1990; Tormen 1998). However, it should be noted that the prediction concerning the small-mass structures is least reliable not only in any PS-like approach, but also in our dynamical approach to the mass function since the validity domain of the Zel'dovich approximation is limited to the high-mass section as explained in § 3.2.

Like the other PS-like formalisms, a normalization factor for the mass function has been introduced, which in our case is 12.5. We have found an approximate solution to our normalization problem with the help of the Jedamzik integral equation for the case of a sharp k-space filter, showing that this rather large normalization factor is due to the low probability of finding a bound region ($\lambda_3 > \lambda_{3c}$) at filtering mass scale M included in an isolated bound region ($\lambda_3 = \lambda_{3c}$) with larger mass M'. But the physical meaning of the sharp k-space filter has yet to be fully understood.

Reproduced with permission of the copyright owner. Further reproduction prohibited without permission.

Chapter 4

Comparison of Analytical Mass Functions with Numerical Simulations

4.1 Introduction

In the previous two Chapters, we have studied two different formalisms for the mass function. One is the classical PS formalism, the other is the new formalism developed recently by Lee & Shandarin (1998, hereafter LS). Basically, the LS formalism adopts the PS statistical concept that bound objects can be counted in terms of filtering a field but replaces the underlying dynamics by choosing more realistic nonspherical collapse condition. The LS formalism has replaced the top-hat spherical model used in the PS formalism by the Zel'dovich approximation, along with the assumption that real virialized bound objects –clumps form from the Lagrangian regions where the gravitational collapse proceeds along all three directions. The resulting LS mass function has been shown to bear a resemblance to the PS one but to look somewhat flatter in shape.

It is true that the LS mass function must be better than the PS one in theory

Reproduced with permission of the copyright owner. Further reproduction prohibited without permission.

since it is based on more realistic nonspherical dynamical model. However it is still quite necessary to test its practical validity by numerical experiments.

In this Chapter, we present the numerical testing results of the LS mass function. We use two fiducial spectral models for this purpose. The first one is the scale free power-law spectrum with spectral index $n = -1$ (it gives a fair approximation to realistic power spectrum around the nonlinear scale $\approx 8h^{-1}$ Mpc for a cold dark matter model, see Fan et al. 1998). The second one is the standard cold dark matter (SCDM) spectrum at four different epochs. The testing result of each comparison reveal that the LS mass function agrees with the numerical data significantly better than the PS one. In § 4.2 we briefly summarize the major points of both the PS and the LS formalisms for the convenience of readers, highlighting the difference and the similarity between the two. In § 4.3 we briefly summarize the N-body simulation used to produce the numerical mass function, and make a comparison between the analytical and the numerical mass functions with the χ^2 estimates. In § 4.4 we discuss the results.

4.2 Summary of Analytic Mass Functions

4.2.1 The PS Mass Function

According to the PS theory, bound objects of mass M form hierarchically in the regions where the linear Gaussian density field $\delta \equiv \rho/\bar{\rho}$ ($\bar{\rho}$: mean density) filtered on a mass scale of M reaches its threshold value δ_c, and their number densities are given by:

$$n_{PS}(M) = \sqrt{\frac{2}{\pi}} \frac{\bar{\rho}}{M^2} \left| \frac{d \ln \sigma}{d \ln M} \right| \frac{\delta_c}{\sigma} \exp\left[- \frac{\delta_c^2}{2\sigma^2} \right]. \tag{4.1}$$

The threshold δ_c for the present epoch is originally given by the spherical top-hat model: $\delta_c \approx 1.69$ (see § 2.2). But in many numerical tests it has been detected that lowered δ_c (roughly 1.5 or even lower) gives a better fit (e.g., Efstathiou &

Reproduced with permission of the copyright owner. Further reproduction prohibited without permission.

Rees 1988; Carlberg & Couchman 1989; Klypin et al. 1995; Bond & Myers 1996). This numerical detection can be understood in the following dynamical argument: Although the top-hat spherical model predicts that the gravitational collapse to "infinite" density occurs when the density reaches $\delta_c \approx 1.69$, clumps in realistic case can form earlier by a rapid virialization process due to the growth of small-scale inhomogeneities (Shapiro, Iliev, & Raga 1998). Actually it is a general tendency in recent N-body simulations for mass functions to set δ_c in the expression of n_{PS} as a free fitting parameter and find the value of δ_c phenomenologically (Monaco 1995 and references therein).

4.2.2 The LS Mass Function

According to the LS formalism (see § 3.2), bound objects with mass M form from the Lagrangian regions where the lowest eigenvalue λ_3 on a filtering scale of M. ($\lambda_3 < \lambda_2 < \lambda_1, \quad \delta = \lambda_1 + \lambda_2 + \lambda_3$) of the deformation tensor d_{ij} (defined as the second derivative of the perturbation potential Ψ such that $d_{ij} = \partial^2\Psi/\partial q_i \partial q_j$, q_i is the Lagrangian coordinate) reaches its threshold λ_{3c} for collapse, and their number densities are given by:

$$n_{LS}(M) = \frac{25\sqrt{10}}{2\sqrt{\pi}}\frac{\bar{\rho}}{M^2}\left|\frac{d\ln\sigma}{d\ln M}\right|\frac{\lambda_{3c}}{\sigma}\left\{\left(\frac{5\lambda_{3c}^2}{3\sigma^2}-\frac{1}{12}\right)\exp\left(-\frac{5\lambda_{3c}^2}{2\sigma^2}\right)\mathrm{erfc}\left(\sqrt{2}\frac{\lambda_{3c}}{\sigma}\right)\right.$$
$$\left.+\frac{\sqrt{6}}{8}\exp\left(-\frac{15\lambda_{3c}^2}{4\sigma^2}\right)\mathrm{erfc}\left(\frac{\sqrt{3}\lambda_{3c}}{2\sigma}\right)-\frac{5\sqrt{2\pi}\lambda_{3c}}{6\pi\sigma}\exp\left(-\frac{9\lambda_{3c}^2}{2\sigma^2}\right)\right\} \quad (4.2)$$

In the original derivation of the LS mass function, the threshold λ_{3c} for collapse has been empirically chosen to be 0.37 as the best value (§ 3.4). The same kind of logic used to give a dynamical explanation to the lowered δ_c of the PS formalism applies here. Although a simple extrapolation of the Zel'dovich approximation to nonlinear regime predicts that the formation of clumps corresponding to the third axis collapse occurs at $\lambda_{3c} = 1$ at the present epoch, the first and the second axis

Reproduced with permission of the copyright owner. Further reproduction prohibited without permission.

collapse speed up the formation of clumps, which would result in a lowered λ_{3c} (see Audit et al. 1997).

In next section, we witness that the LS mass function with the originally suggested value of $\lambda_3 = 0.37$ does agree with the experimental results very well.

4.3 Numerical vs. Analytical Mass Functions

The numerical data for the case of a power law spectrum presented here have been kindly provided by Tormen (1998). He produced his numerical mass function from a large N-body simulation of an flat matter-dominated universe for a scale free power spectrum $P(k) \propto k^n$ with a spectral index $n = -1$, which has been performed by White (1994) using Particle-Particle-Particle-Mesh code (Efstathiou et al. 1985) with 100^3 particles in a 256^3 mesh and a periodic boundary condition. The dimensionless Hubble constant adopted in the simulation is $h = 0.5$, and the power spectrum is normalized to match the observed local abundance of galaxy clusters (White et al. 1993).

Tormen (1998) identified the gravitationally bound clumps (dark halos) from the simulations with the friends-of-friends algorithm with a linking length 0.2 [Davis et al. 1985, hereafter FOF (0.2)]. He obtained numerical mass functions using the FOF (0.2) algorithm for 10 different output times coming from two different N-body realizations of the same initial conditions. And then he took an average over 10 output values to produce a final average numerical mass function with poissonian error bars for each FOF (0.2) clumps. As explained clearly in §3 of Tormen (1998), the average process over 10 outputs were performed by weighting each contribution from 10 outputs in each mass range by the number of clumps belonging to that mass range (Lacey & Cole 1994). Here we compare the analytical mass functions with the final average numerical results.

It is sometimes useful to define a filter-depending nonlinear mass scale M_* related to the characteristic mass M_0 by $M_* \equiv M_0(\delta_c)^{-6/(n+3)}$ for a dimensionless

Reproduced with permission of the copyright owner. Further reproduction prohibited without permission.

rescaled mass variable M/M_* for power-law spectrum case. Tormen (1998) used a top-hat filter with fixed $\delta_c = 1.69$ to calculate M_* whose value was given by $6.16 \times 10^{13} M_\odot$. Note that $\sigma(M_*) = \delta_c$ since $\sigma(M_0) = 1$. Figure 4.1 shows the comparison results for a power law spectrum case. Obviously the LS mass function agrees with the numerical data much better than the PS one. Especially in the high mass section ($M > M_*$) the fit between the LS and the numerical mass function is remarkably excellent.

For the case of SCDM spectrum, we use the halo catalog provided by Governato et al. (1998) to produce numerical mass functions. And for the shape of the SCDM power spectrum, Governato et al. (1998) chose the one given by Bardeen et al. (1986) with $\Omega = 1$ and $h = 1$ (see §5.2). They performed N-body simulations with the simulation box size of $500h^{-1}$Mpc and the periodic boundary conditions to match the forthcoming Sloan Digital Sky Survey. The high mass resolution was guaranteed in terms of 47 million particles. They ran the simulation for four different epochs; $z = 0, 0.43, 1.14$ and 1.86. The output from each epoch was rescaled by changing the present day value of the corresponding rms fluctuations; $\sigma = 1, 0.7, 0.467$ and 0.35. FOF (0.2) was also used as a halo finder. See Governato et al. (1998) for a detailed description of the N-body simulation used to produce the halo catalogs.

Figure 4.2 shows the comparison results for the SCDM case. Again the LS mass function fits with the numerical data much better than the PS one.

We compute the χ^2 to quantify the testing results of analytical mass function against numerical data, (n_i, M_i):

$$\chi^2 = \sum_{i=1} \left[\log_{10} n_i - \log_{10}[n(M_i; \lambda_{3c} \text{or} \delta_c)] \right]^2 . \tag{4.3}$$

Table 4.1 shows the obtained values of χ^2 for each LS and PS mass function. As one can read, the value of χ^2_{LS} is lower than that of χ^2_{PS} by a factor of 10 for each case. In other words, the LS mass function agrees with the numerical

Reproduced with permission of the copyright owner. Further reproduction prohibited without permission.

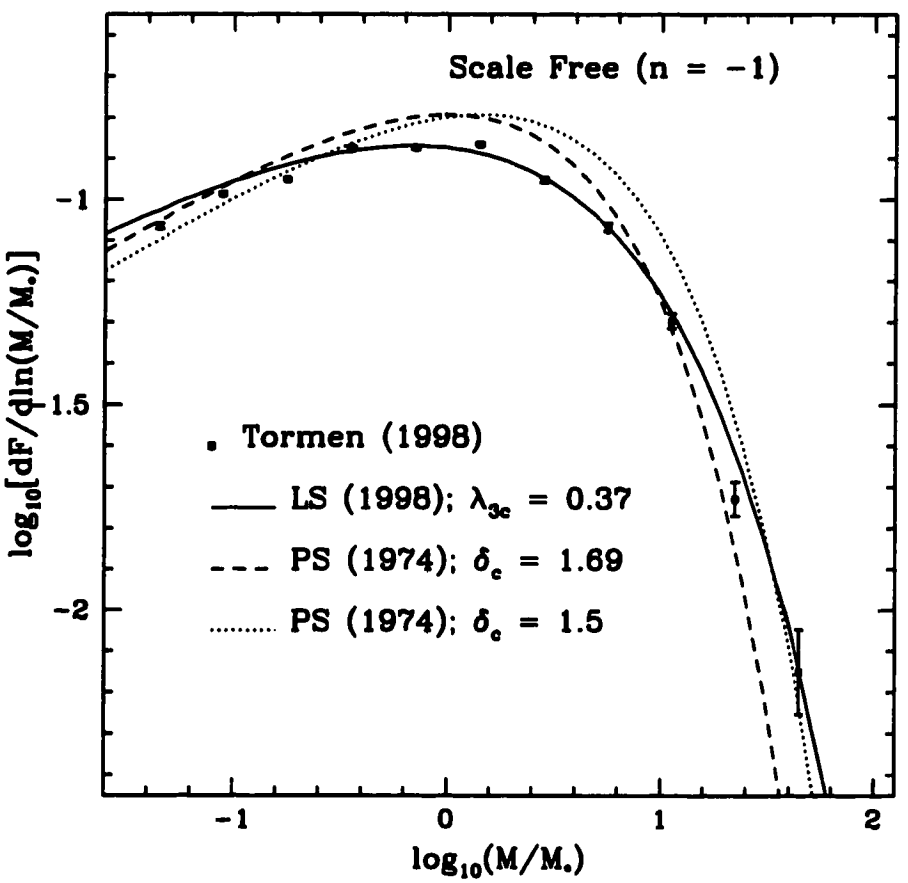

Figure 4.1: The square dots correspond to the numerical mass function averaged over 10 output results from two N-body realizations using the FOF (0.2) algorithm for the case of a n=-1 power-law spectrum. Here $dF/d\ln M = (M^2/\bar{\rho})n(M)$. The error bars are poissonian. See also the top left panel of Fig.2 in Tormen (1998). The solid line stands for the LS mass function with $\lambda_{3c} = 0.37$ while the dashed and the dotted lines represent the PS mass function with $\delta_c = 1.69$ and 1.5 respectively.

Reproduced with permission of the copyright owner. Further reproduction prohibited without permission.

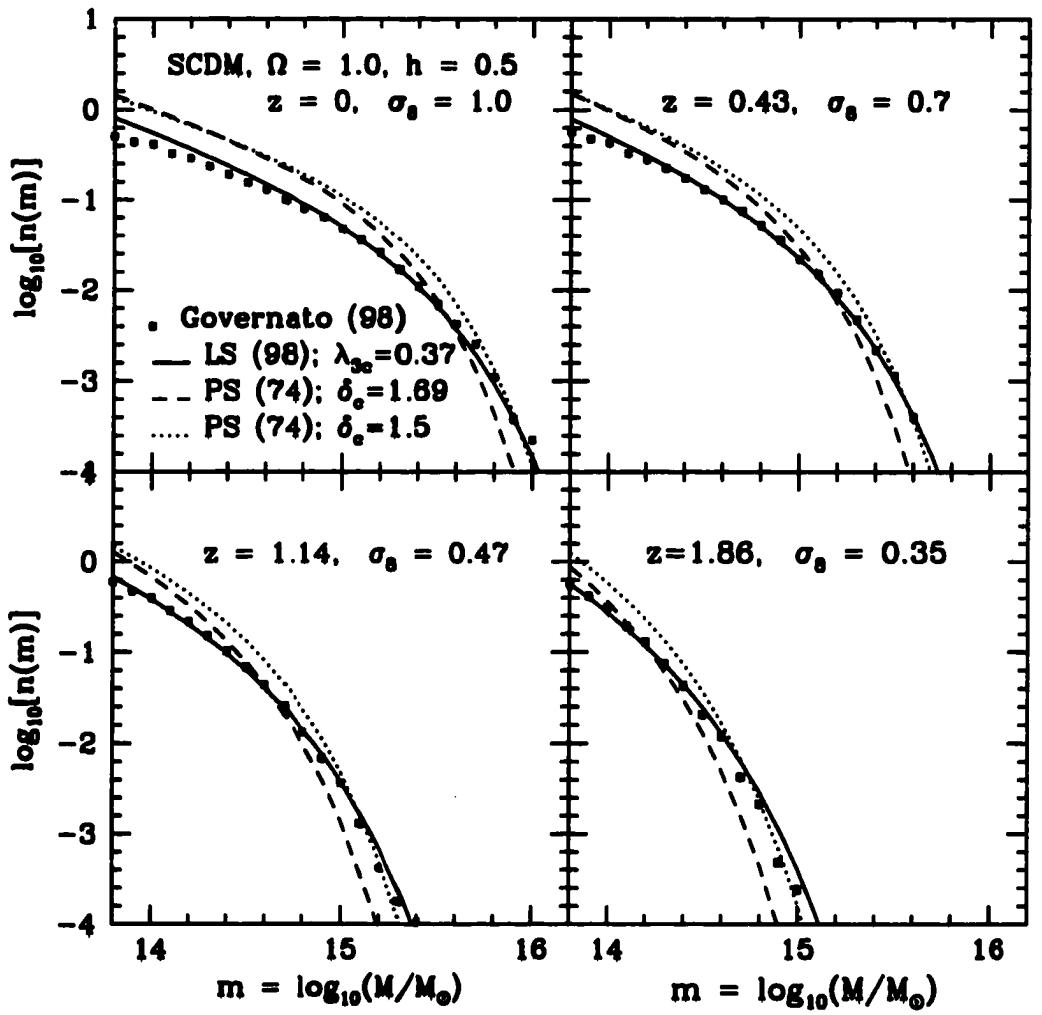

Figure 4.2: The square dots correspond to the numerical mass function obtained from halo catalogs produced by one N-body realization using the FOF (0.2) algorithm at four different epochs for the case of SCDM model. The solid line stands for the LS mass function with $\lambda_{3c} = 0.37$ while the dashed and the dotted line represent the PS mass function with $\delta_c = 1.69$ and 1.5 respectively.

Reproduced with permission of the copyright owner. Further reproduction prohibited without permission.

Table 4.1: The values of χ^2 for the LS and the PS mass functions

model	χ^2_{LS}	χ^2_{PS}
Scale Free (n=-1)	0.01	0.10
SCDM (z=1.00)	0.14	3.13
SCDM (z=0.43)	0.17	4.05
SCDM (z=1.14)	0.12	5.70
SCDM (z=1.86)	0.24	2.79

results much better than the PS one in a respect that the discrepancy between the analytical and the numerical results is reduced by a factor of 10.

4.4 Discussion

Although the PS mass function has been traditionally used to predict the number densities of gravitationally collapsed objects for last two decades, recent high resolution simulations found that it is not very accurate tool (Tormen 1998; Governato et al. 1998). Moreover, the recent wealth of observations on low and high-redshift objects is calling for a more accurate description of the mass function than was needed in the past.

To make the PS mass function work better, several ad-hoc assumptions and modifications on the PS theory have been made. For example, Governato et al. (1998) suggested that the density threshold be a function of redshift, i.e., $\delta_c(z)$, and provided a fitting formula for $\delta_c(z)$. Sheth & Tormen (1999) gave a similar idea that the threshold is a function of mass $\delta_c(M)$, finding also a phenomenological fitting formula. But these ad-hoc assumptions themselves point out the weakness of the PS theory since there is no physical meaning to these assumptions. It may make the PS mass function fit better with the numerical data but it degrades the PS mass function to a pure phenomenological device without physical foundations.

Thus it is essential to have a new improved alternative of the PS one. In this

Reproduced with permission of the copyright owner. Further reproduction prohibited without permission.

chapter, we test one possibility; we have numerically tested an analytical mass function recently derived by Lee & Shandarin (1998a) and compared the results with that of the PS one.

The LS formalism is a dynamically improved version of the PS formalism. In other words, it is not just a modified fitting formula of the PS mass function but it is derived from better physical background than the PS one. The gravitational clustering in the LS formalism is described by a realistic nonspherical dynamical model based on the Zel'dovich approximation. Consequently it deals with the λ_3-field instead of the δ-field in the PS formalism, with the LS mass function being characterized by the threshold λ_{3c} while the PS by δ_c. Furthermore N-body simulations demonstrated a strong correlation between the peaks of the λ_3-field and the final locations of bound objects (Shandarin & Klypin 1984) while detecting a poor correlation between the peaks of the δ-field and the final locations of bound objects (Katz, Quinn, & Gelb 1988).

The testing results obviously have revealed that the LS mass function with consistent value of $\lambda_{3c} = 0.37$ is significantly better than the PS one with $\delta_c = 1.69, 1.5$ in fitting to the numerical data in the whole mass section for all tested epochs. The consistency of the threshold λ_{3c} indicates how well the LS mass function behaves as a better alternative should be, given that the threshold δ_c of the PS mass function had to be changed from epoch to epoch to give a good fit.

Given the excellent fitting results of the LS mass function demonstrated here, we expect that the LS mass function will provide a more accurate statistical tool than the PS one to study the formation of the large-scale structure, and suggest that the LS theory be tested widely and applied to various areas like the PS theory.

Reproduced with permission of the copyright owner. Further reproduction prohibited without permission.

Chapter 5

Large Scale Biasing and the Primordial Gravitational Potential

5.1 Introduction

The PS-like formalism for the mass function provides a good statistical technique for calculating the number densities of bound objects as shown in Chapter 4. However one drawback of any PS-like formalism is that it gives the average number densities of bound objects, assuming that the structures are distributed randomly. Therefore it fails in predicting in which way the cosmic nonlinear structures are really distributed. This Chapter addresses this issue by highlighting the role of the primordial gravitational potential on the structure formation.

Some effect of the primordial gravitational potential upon the structure formation has been already noted. Kofman & Shandarin (1988) have noticed that the adhesion approximation [1] predicts that the formation of voids is associated with

[1]The adhesion approximation is a extension of the Zel'dovich approximation with a viscosity term added to mimic the nonlinear gravitational force (Shandarin 1994)

Reproduced with permission of the copyright owner. Further reproduction prohibited without permission.

positive peaks of the primordial gravitational potential. Sahni, Sathyaprakash, & Shandarin (1994) studied the effect and measured a significant correlation between the sizes of voids and the value of primordial gravitational potential in numerical simulations of the adhesion model. By investigating the evolution of correlation between the potential and the density perturbations, Buryak, Demianski, & Doroshkevich (1992) showed that the formation of super large scale structures is mainly determined by the spatial distribution of the gravitational potential. Recently, Madsen et al. (1997) have demonstrated by N-body simulations that the under dense and the over dense regions are closely linked to the regions with the positive and the negative gravitational potential respectively. Thus, given all these results showing the important role of the primordial gravitational potential in the structure formation, it would be interesting to calculate the effect of the primordial potential upon the mass distribution function.

In this Chapter we investigate and show how much the primordial gravitational potential φ affects the mass distribution function of galaxy clusters. Modifying the PS formalism, we derive a constrained mass distribution function $n(M|\varphi)$ defined as the comoving number densities of clumps of mass M in the regions where the primordial gravitational potential fluctuation satisfies some specified conditions ($\varphi < -\varphi_c, \varphi > \varphi_c$ with $\varphi_c > 0$: constant). The Cold Dark Matter model (CDM) with $\Gamma \equiv \Omega h = 0.25$ normalized by $\sigma_{TH}(8h^{-1}\mathrm{Mpc}) = 1$ is used to demonstrate the significance of the effect.

5.2 Constrained Mass Functions

In order to incorporate the primordial gravitational potential fluctuations term into the PS formula, we first have to derive the conditional probability density distribution $p(\delta|\varphi < -\varphi_c)$. First of all let us find the two point Gaussian distribution,

Reproduced with permission of the copyright owner. Further reproduction prohibited without permission.

$p(\delta, \varphi)$:

$$p(\delta,\varphi) = \frac{1}{2\pi\sqrt{\sigma_\delta^2\sigma_\varphi^2 - \sigma_v^4}} \exp\Big\{ -\frac{\sigma_\varphi^2}{2(\sigma_\delta^2\sigma_\varphi^2 - \sigma_v^4)}\delta^2 - \frac{\sigma_v^2}{(\sigma_\delta^2\sigma_\varphi^2 - \sigma_v^4)}\delta\varphi - \frac{\sigma_\delta^2}{2(\sigma_\delta^2\sigma_\varphi^2 - \sigma_v^4)}\varphi^2 \Big\} \tag{5.1}$$

where σ_δ^2, σ_v^2, σ_φ^2 are the density, the velocity, and the potential variance respectively. Here the velocity variance is related to δ and φ by $< \delta\varphi >= -\sigma_v^2$.

Now $p(\delta|\varphi < -\varphi_c)$ can be obtained by

$$\begin{aligned} p(\delta|\varphi < -\varphi_c) &= \frac{p(\delta, \varphi < -\varphi_c)}{p(\varphi < -\varphi_c)} = \frac{\int_{-\infty}^{\varphi_c} p(\delta,\varphi)d\varphi}{\int_{-\infty}^{\varphi_c} p(\varphi)d\varphi} \\ &= \frac{1}{\sqrt{2\pi}\sigma_\delta} \exp\Big(-\frac{\delta^2}{2\sigma_\delta^2}\Big)\Big[1 - \mathrm{erf}\Big(\frac{\varphi_c}{\sqrt{2}\sigma_\varphi}\Big)\Big]^{-1} \times \\ &\quad \Big[1 + \mathrm{erf}\Big(\frac{\kappa\frac{\delta}{\sigma_\delta} - \frac{\varphi_c}{\sigma_\varphi}}{\sqrt{2(1-\kappa^2)}}\Big)\Big]. \end{aligned} \tag{5.2}$$

Here $p(\varphi)$ is a Gaussian distribution same as equation (2.19) but δ and $\sigma_\delta(M)$ replaced by φ and σ_φ. The other conditional probability density distribution function $p(\delta|\varphi > \varphi_c)$ has the same form as equation (5.2) except for the opposite sign in front of the second error function term.

In the case of a sharp k-space filter assumed throughout this Chapter, σ_δ^2, σ_v^2 and σ_φ^2 are given as

$$\sigma_\delta^2(M) = \frac{1}{2\pi^2}\int_0^{k_c(M)} dk k^2 P(k), \tag{5.3}$$

$$\sigma_v^2(M) = \frac{1}{2\pi^2}\int_0^{k_c(M)} dk P(k), \tag{5.4}$$

$$\sigma_\varphi^2 = \frac{1}{2\pi^2}\int_{k_l}^{\infty} dk k^{-2} P(k). \tag{5.5}$$

It is worth noting that the variances σ_δ^2 and σ_v^2 depend on the sharp k-space cutoff $k_c = (M/6\pi^2)^{-1/3}$, but the variance of the primordial potential, σ_φ^2 does not.

Reproduced with permission of the copyright owner. Further reproduction prohibited without permission.

We are interested in evaluating the effect of the *primordial* potential fluctuations and thus take σ_φ without filtering. The long wave cutoff $k_l^{-1} \approx 3000h^{-1}$Mpc corresponds to the assumption that the waves longer than the cosmological horizon are irrelevant to the processes on scales of the structures in the universe (i.e. smaller than a few hundred of h^{-1}Mpc). A particular choice of k_l is unimportant since σ_φ^2 depends on $1/k_l$ only logarithmically for the Harrison-Zel'dovich spectrum described below.

As a result of the incorporation of the potential into the probability density distribution, the volume fraction $F(M)$ in the PS formula is now a function of both σ_δ and σ_v each of which in turn is a function of mass M:

$$F(M) = F[\sigma_\delta(M), \sigma_v(M)] = \int_{\delta_c}^{\infty} d\delta \; p(\delta|\varphi < -\varphi_c). \tag{5.6}$$

Now the constrained mass function $n(M|\varphi < -\varphi_c)$ can be derived as

$$n(M|\varphi < -\varphi_c) = \frac{\bar{\rho}}{M}\left|\frac{\partial F}{\partial \sigma_\delta}\frac{d\sigma_\delta}{dM} + \frac{\partial F}{\partial \sigma_v}\frac{d\sigma_v}{dM}\right|. \tag{5.7}$$

We find the differential volume fraction $\partial F/\partial\sigma_\delta$ and $\partial F/\partial\sigma_v$ analytically:

$$\begin{aligned}
\frac{\partial F}{\partial \sigma_\delta} &= \frac{A\delta_c}{\sqrt{2\pi}\sigma_\delta^2}\exp\left(-\frac{\delta_c^2}{2\sigma_\delta^2}\right)\left\{1+\mathrm{erf}\left[\frac{\sigma_v^2}{\sqrt{2(\sigma_\delta^2\sigma_\varphi^2-\sigma_v^4)}\sigma_\delta}\left(\delta_c-\frac{\sigma_\delta^2}{\sigma_v^2}\varphi_c\right)\right]\right\} \qquad (5.8)\\
&\quad -\frac{A\sigma_v^2}{\pi\sqrt{\sigma_\delta^2\sigma_\varphi^2-\sigma_v^4\sigma_\delta}}\exp\left(-\frac{\varphi_c^2}{2\sigma_\varphi^2}\right)\\
&\qquad \times\exp\left[-\frac{\sigma_\varphi^2}{2(\sigma_\delta^2\sigma_\varphi^2-\sigma_v^4)}\left(\delta_c-\frac{\sigma_v^2}{\sigma_\varphi^2}\varphi_c\right)^2\right], \qquad (5.9)\\
\frac{\partial F}{\partial \sigma_v} &= \frac{2A\sigma_v}{\pi\sqrt{\sigma_\delta^2\sigma_\varphi^2-\sigma_v^4}}\exp\left(-\frac{\varphi_c^2}{2\sigma_\varphi^2}\right)\times\\
&\quad \exp\left[-\frac{\sigma_\varphi^2}{2(\sigma_\delta^2\sigma_\varphi^2-\sigma_v^4)}\left(\delta_c-\frac{\sigma_v^2}{\sigma_\varphi^2}\varphi_c\right)^2\right]\mathrm{erfc}\left[\frac{\varphi_c}{\sqrt{2}\sigma_\varphi}\right], \qquad (5.10)
\end{aligned}$$

Reproduced with permission of the copyright owner. Further reproduction prohibited without permission.

where

$$A = \left[1 - \mathrm{erf}\left[\frac{\varphi_c}{\sqrt{2}\sigma_\varphi}\right]\right]^{-1}. \tag{5.11}$$

To compute $d\sigma_\delta/dM$ and $d\sigma_v/dM$, the functional form of the power spectrum $P(k)$ first should be specified. In the previous Chapters we have used simple scale free power law spectra $P(k) \propto k^n$ for mathematical convenience. But in order to demonstrate the significance of the effect of the primordial gravitational potential on the structure formation, we had better use a realistic power spectrum although it may complicate the calculation.

According to the inflation theory, the primordial density fluctuations assumed a power law spectrum $P(k) \propto k^n$ with $n = 1$. This spectrum is called the Harrison-Zel'dovich spectrum and generally believed to be the case for the initial power spectrum. Since then the nonlinear evolution of the density fluctuations has changed the shape of $P(k)$ which form has been determined empirically. Here we adopt the following power spectrum given by Bardeen et al. (1986):

$$P(k) \propto k\left[\frac{\ln(1+2.34q)}{2.34q}\right]^2 [1 + 3.89q + (16.1q)^2 + (5.46q)^3 + (6.71q)^4]^{-1/2}, \tag{5.12}$$

where $q = k/\Gamma$ and k is measured in units of $h\mathrm{Mpc}^{-1}$. For the normalization of $P(k)$, we follow the *conventional* scheme such that $\sigma_\delta(8h^{-1}\mathrm{Mpc})$ is set to be unity with a top-hat filter [see equation (1.19)], which is also in agreement with the COBE measurements for the CDM model with $\Gamma = 0.25$ (see Peacock & Dodds 1994). The above power spectrum is plotted in Figure 5.1.

With the given power spectrum, we finally derive the constrained mass function $n(M|\varphi < -\varphi_c)$ through equations (5.6)-(5.12). Figure 5.2 shows the magnitude of the effect in terms of the cumulative mass functions. The upper panel shows the cumulative conditional mass functions $n(> M|\varphi < -\varphi_c)$ and $n(> M|\varphi > \varphi_c)$ (for each case of $\varphi_c = \sigma_\varphi, 0$) along with the unconditional PS mass function, $n(> M)$. The cumulative mass functions were obtained by integrating the mass functions

Reproduced with permission of the copyright owner. Further reproduction prohibited without permission.

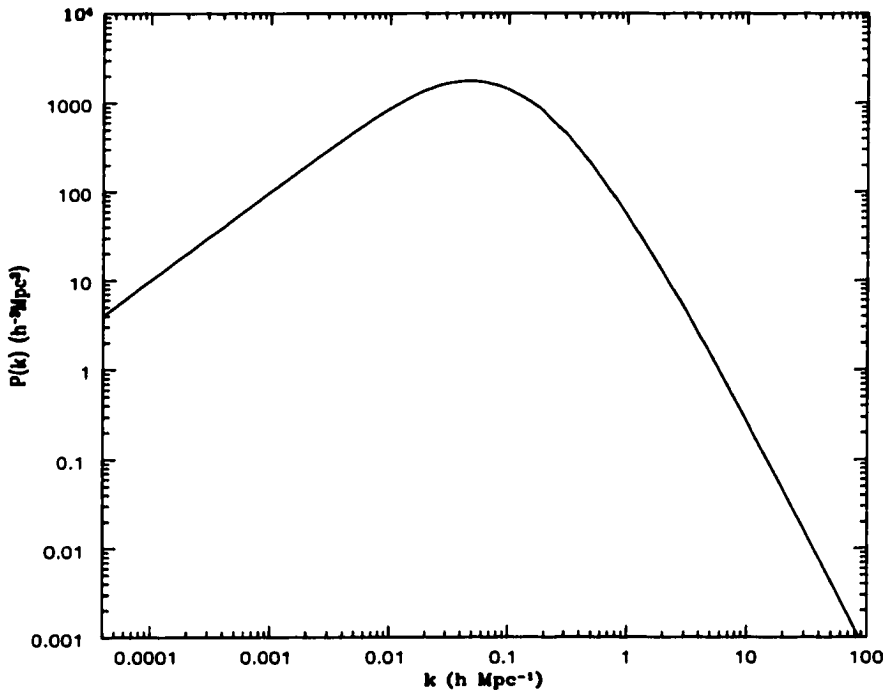

Figure 5.1: The power spectrum for the CDM model with $\Gamma = 0.25$ normalized by $\sigma_\delta(8h^{-1}\mathrm{Mpc}) = 1$.

$n(M|\varphi < -\varphi_c)$ numerically. The shaded area shows the fit to the observational mass function of rich clusters given by Bahcall & Cen (1993). The ratios of the conditional mass functions to the unconditional one are plotted in the lower panel of Figure 5.2.

We also calculate the probability that a clump with mass M is located in the potential regions satisfying the chosen condition, for instance, $\varphi < -\varphi_c$

$$P(\varphi < -\varphi_c|M) = \frac{n(M|\varphi < -\varphi_c)}{n(M)} P(\varphi < -\varphi_c), \tag{5.13}$$

where $P(\varphi < -\varphi_c)$ is the fraction of space satisfying the given condition (see figure 5.3). The other probabilities $P(-\varphi_c < \varphi < 0|M)$, $P(0 < \varphi < \varphi_c|M)$, and $P(\varphi_c < \varphi|M)$ can be obtained in a similar manner.

Reproduced with permission of the copyright owner. Further reproduction prohibited without permission.

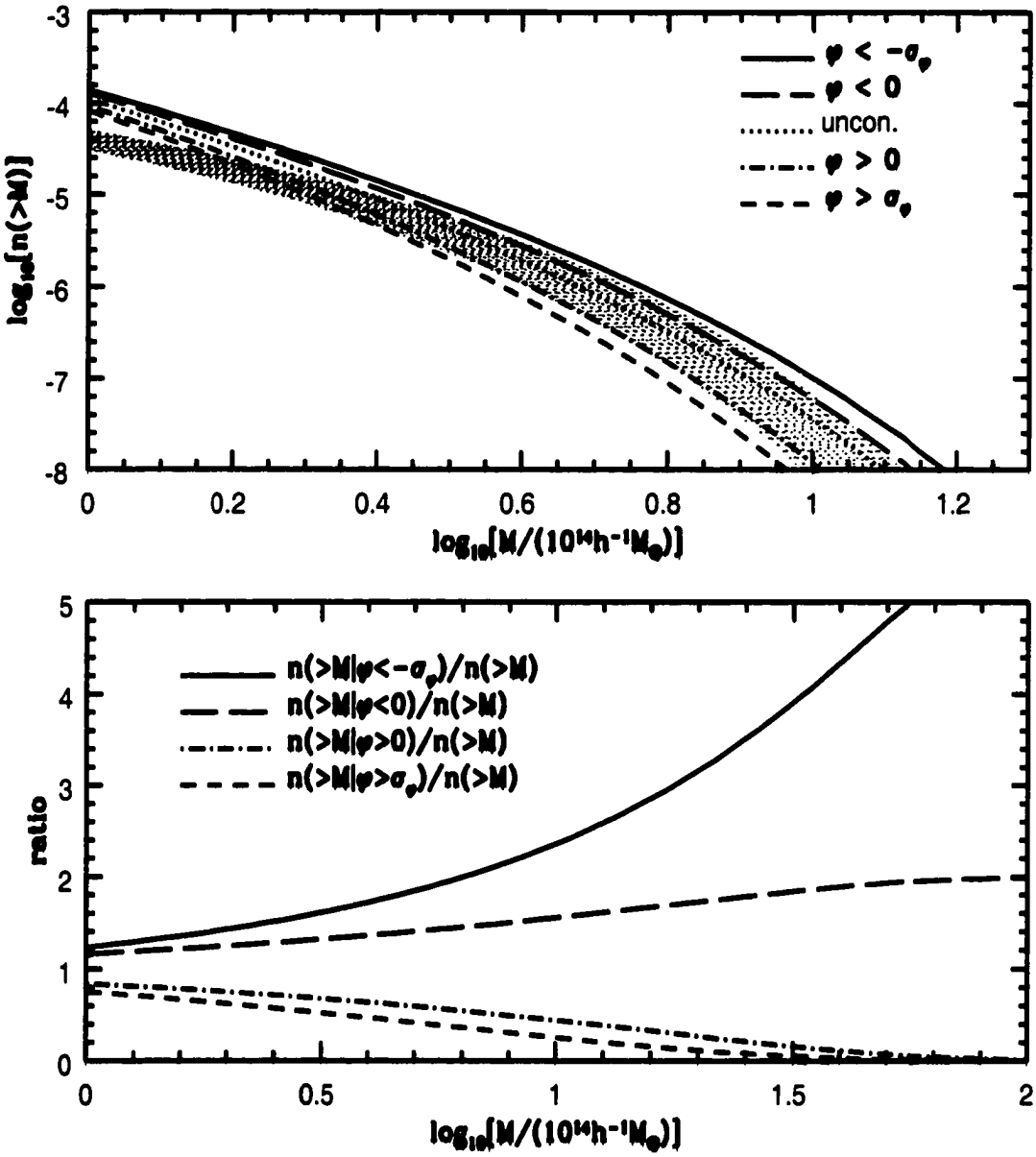

Figure 5.2: In the upper panel the conditional cumulative mass function satisfying chosen potential condition is plotted. The solid, the long dashed, the dot-dashed, and the dashed lines correspond to the conditions $\varphi < -\sigma_\varphi$, $\varphi < 0$, $\varphi > 0$, and $\varphi > \sigma_\varphi$ respectively, while the dotted line represents the unconditional cumulative PS mass function. The shaded area is 1σ fit to the observational cumulative mass function of rich clusters by Bahcall and Cen (1993). In the lower panel the ratio of the conditional cumulative mass functions to the unconditional one is plotted for each condition. The CDM spectrum with $\Gamma = 0.25$ normalized to $\sigma_\delta(8h^{-1}\mathrm{Mpc}) = 1$ has been used.

Reproduced with permission of the copyright owner. Further reproduction prohibited without permission.

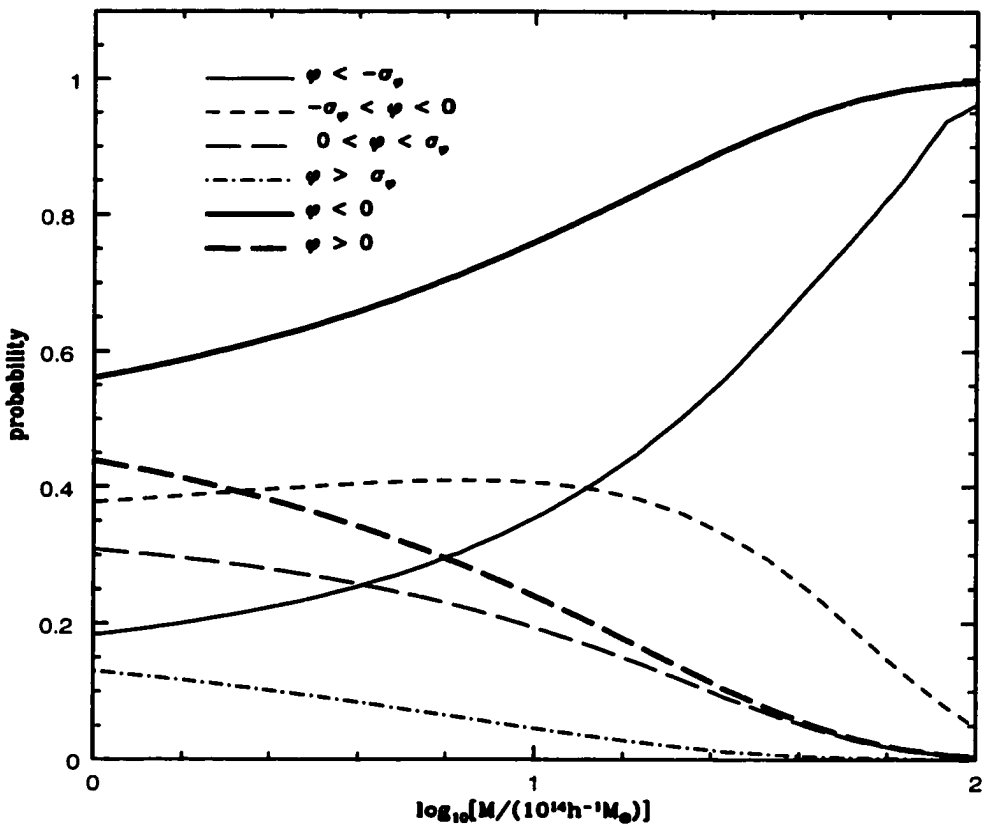

Figure 5.3: The probability that a clump with mass M can be found in the regions satisfying chosen potential condition is plotted. The heavy solid, the heavy dashed, the solid, the dashed, the long dashed, and the dot-dashed lines correspond to the condition $\varphi < 0$, $\varphi > 0$, $\varphi < -\sigma_\varphi$, $-\sigma_\varphi < \varphi < 0$, $0 < \varphi < \sigma_\varphi$, and $\varphi > \sigma_\varphi$ respectively.

5.3 Discussion

The PS formalism has been proved to be a simple but very effective tool widely used for constraining cosmological models. We have modified it by considering the dependence of mass function on the initial perturbation of gravitational potential. The resulting modified PS theory predicts that the clumps with masses greater than roughly $10^{14}h^{-1}M_\odot$ have a noticeable tendency to form in the troughs of the primordial gravitational potential (the regions where the primordial poten-

Reproduced with permission of the copyright owner. Further reproduction prohibited without permission.

tial fluctuations were negative). This quantitative prediction can be tested in large N-body simulations. Regardless of the outcome it will shed light on the PS formalism; if our prediction is confirmed, it will show a new potency of the PS technique. Otherwise a new limitation to the formalism will be established.

Assuming that the prediction is correct at least qualitatively, [2] we would like to discuss some of its obvious consequences. The scale of the initial potential

$$R_\varphi = \sqrt{3}\sigma_\varphi/\sigma_{\varphi'} = \sqrt{3\frac{\int_{k_l}^{\infty} dk k^{-2} P(k)}{\int_0^{\infty} dk P(k)}} \approx 120 h^{-1}\mathrm{Mpc} \qquad (5.14)$$

does not depend on any ad hoc scale; the dependence on k_l is extremely weak ($\propto \sqrt{ln(1/k_l)}$ for the Harrison-Zel'dovich spectra assumed here). Perhaps, it is worth mentioning that the scale of the potential is also practically independent of the smoothing scale unless it exceeds the value of a few tens of h^{-1}Mpc. The density scale $R_{\delta_{k_c}}$ is determined by the scale of the smoothing window function k_c that has only one "natural" scale corresponding nonlinearity $k_c = k_{nl}$. For the model in question the scale of the primordial potential is found to be $R_\varphi \approx 120 h^{-1}$Mpc. The scale of the density contrast field reaches this value $R_\delta = \sqrt{3}\sigma_\delta/\sigma_{\delta'} \approx 120 h^{-1}$Mpc only after it is smoothed on $k_c \approx 0.017 h\mathrm{Mpc}^{-1}$. The corresponding density variance on this scale is $\sigma_\delta(0.017 h\mathrm{Mpc}^{-1}) \approx 0.03$. On the other hand, the number of clumps with masses $10^{14} - 10^{15} h^{-1} M_\odot$ can easily be 30% greater in the troughs of the potential than the mean density $n(>M) = 0.5[n(>M|\varphi<0) + n(>M|\varphi>0)]$ (see Figure 5.1). Thus, the bias factor b (defined by the relation $\Delta n_{cl}/n_{cl} = b\Delta\rho_m/\rho_m$) reaches at least 10 on the scale about $120 h^{-1}$Mpc.

Qualitatively the bias phenomenon can be explained as follows. The initial density contrast is proportional to the Laplacian of the initial potential ($\delta \propto \nabla^2\varphi$). Therefore the two fields are cross-correlated: the positive peaks of δ are more likely

[2] N-body simulations (e.g., Madsen et al. 1997) and the adhesion model (Sahni et al. 1994) have already visually demonstrated this bias effect of the gravitational potential.

Reproduced with permission of the copyright owner. Further reproduction prohibited without permission.

to be found in the troughs of the potential where it is negative. The correlation is not very strong (for $k_c = 0.25h\text{Mpc}^{-1}$ corresponding to $\sigma_\delta = 1$ the crosscorrelation coefficient $\kappa = \sigma_v^2(0.25h\text{Mpc}^{-1})/\sigma_\varphi\sigma_\delta(0.25h\text{Mpc}^{-1}) \approx 0.12$). But the clusters are extreme objects corresponding to the tail of the mass function, and thus very sensitive to the environment. That is why the clusters put one of the strongest constraints on cosmological models (Klypin & Rhee 1994; Bond & Myers 1996; Fan et al. 1998; Bahcall & Fan 1998).

Incorporating the motion of mass into dynamics can only increase the bias effect due to the nonlinear effects although they are quite small on the scale in question. But, the point is not in the magnitude of the nonlinear effects but rather in their sign. On the scale of the potential the mass moves from the peaks of the potential to the troughs. Using the Zel'dovich approximation one can easily estimate the rms displacement of the mass on the scale of the potential (Shdandarin 1993):

$$d_{rms} = \sqrt{\frac{\int_0^{0.017h} P(k)dk}{\int_0^{0.25h} P(k)k^2dk}} \approx 3h^{-1}\text{Mpc}. \qquad (5.15)$$

It is relatively small compared to the scale of the potential but coherent on the scale of the potential field, and therefore it can only enhance the bias effect. Another nonlinear effect is related to the rate of growth of perturbations. For the perturbations on the scale of a few Mpc the potential troughs/peaks may be viewed as patches with slower/faster expansion rate that corresponds to the increase/decrease of the rate of growth of small-scale perturbations. Similarly, the bias is enhanced in the redshift space because the velocity field is directed toward the troughs and away from peaks of the potential. Both effects can increase the bias by about 5% depending on the initial spectrum.

Another way of calculating the constrained mass function would be using the peak-background split technique suggested by Kaiser (1984) to explain the en-

Reproduced with permission of the copyright owner. Further reproduction prohibited without permission.

hanced correlation function of rich clusters. Obviously, the initial potential resembles the smoothed initial density field if the filter has a sufficiently large scale, but the former is never identical to the latter. The potential itself can be viewed as a smoothed density field with a very soft scale-free filter $W(k) \propto k^{-2}$. Typically the density field is filtered with much harder filters (e.g. top-hat, Gaussian, or sharp k-space filters), that impose the scale which is an ad hoc parameter. The magnitude of the bias in our approach is determined by the crosscorrelation of the density contrast smoothed at the scale (k_c) of nonlinearity ($\sigma_{\delta_{k_c}} = 1$) with the initial potential that does not have any ad hoc parameters. Probably, the value of the crosscorrelation coefficient determines the bias in the peak-split approach as well. The crosscorrelation of the density field δ_{k_c} smoothed on the scale of nonlinearity ($k_c = 0.25h\mathrm{Mpc}^{-1}$) with the field δ_{k_φ} smoothed on the scale of the potential ($k_\varphi = 0.017h\mathrm{Mpc}^{-1}$) is about 4 times weaker than the correlation of δ_{k_c} with the initial potential φ. Thus, we expect that the bias of galaxy clusters on such large scales as the scale of the initial potential ($\approx 120h^{-1}\mathrm{Mpc}$) is stronger toward the troughs of the potential fluctuations rather than to the peaks of the density fluctuations δ_{k_c} smoothed with the corresponding filter. We have not applied the split peak-background approach because it is not clear how to avoid arbitrariness in choosing the scale that splits the density into small-scale peaks and large-scale background field. This question requires a separate study.

Applying this effect to observations one has to take into account the following issues. The gravitational potential does not evolve much on large scales especially in the Einstein-de Sitter universe (Kofman & Shandarin 1988; Pauls & Melott 1995; Melott, Sathyaprakash, & Sahni 1996). Therefore, the potential at present is very similar to the primordial one on scales much greater than the scale of nonlinearity. A simple explanation to this in the frame of the standard scenario of the structure formation is due to the fact that the mass has been displaced by the distance about $10h^{-1}\mathrm{Mpc}$ (Shandarin 1993). Therefore, the potential on

Reproduced with permission of the copyright owner. Further reproduction prohibited without permission.

scales greater than, say, $30h^{-1}$Mpc has been changed very little.

Clusters can be used as *statistical* tracers of the potential. In addressing this question it is worth noting that the shot noise is an important factor since clusters are rare objects. Using the observational mass function (Bahcall & Cen 1993) one can estimate that an average spherical patch of the radius $\approx 60h^{-1}$Mpc contains about 30 clusters with the masses greater than $10^{14}h^{-1}M_{\odot}$. Thus, the shot noise is about 18% on this scale which is comparable with the bias itself (see Figure 5.1, the bottom panel). However, Figure 5.2 suggests that the most massive clusters $[M > 10^{15}h^{-1}M_{\odot}]$ are very likely to reside in the regions of negative potential ($P > 75\%$) and very unlikely in the regions of high potential ($P < 5\%$ if $\varphi > \sigma_{\varphi}$). More detailed analysis will be present elsewhere.

Probably, the best candidates for the markers of the troughs in the field of the primordial potential fluctuations are superclusters (defined as clusters of clusters) (Bahcall & Soneira 1984) especially with highest density enhancements (Shapley supercluster) and the giant geometrical patterns in the cluster distribution (Tully et al. 1992).

Reproduced with permission of the copyright owner. Further reproduction prohibited without permission.

Chapter 6

Concluding Remarks

In this thesis we have developed analytical formalisms for the cosmic mass function with the classical PS theory as a foothold. We dynamically improved the PS theory by choosing a nonspherical underlying dynamics and derived a new (LS) mass function which turns out to work much better than the PS one in numerical tests. We also modified the PS theory to study the role of the primordial gravitational potential on the formation of galaxy clusters and measured the large scale biasing effect quantitatively.

The excellent testing result of the LS mass function motivates us to apply it to diverse topics. First, although we focused on the matter-dominated flat universe ($\Omega = 1$) at present epoch in the original derivation of the LS mass function, it will be interesting to apply the LS formalism to $\Omega < 1$ universe at earlier epoch and to investigate the evolution rate of the LS mass function. Compared with the observational data, it will play a part to determine the value of Ω more accurately (Fan et al. 1997). Second, the LS formalism will be able to provide a merging history of dark halos in a proto-cluster environment. Lacey & Cole (1993) found an analytical method to describe the merger of halos by using the extended PS mass function (Bond et al. 1991) which relates the number densities of halos at two different epochs. But Tormen (1998) recently showed that the

Reproduced with permission of the copyright owner. Further reproduction prohibited without permission.

PS theory cannot describe the global evolution of clustering and its evolution in a proto-cluster environment by comparing the PS and the extended PS mass functions with the numerical results. He noted that the discrepancy between the PS theory and the N-body results is in the sense that the PS theory underpredicts the number densities of high-mass proto-clusters at high redshift. This numerical detection implies that the PS formalism is not quite appropriate for describing the merger history of progenitor halos. I believe that it is due to the structural failure of the PS formalism originated by the departure of true collapse from spherical one (Governato et al. 1998). As shown previously (§ 4.3), the LS mass function is flatter than the PS one in the high mass-section, that is, the LS theory predicts more high-mass objects. And this tendency should be stronger at higher redshifts. I expect that the extended LS mass function will give us a new theoretical insight into the evolution of gravitational clustering even in a proto-clustering environment. In addition the LS theory will be more useful in predicting gravitational lensing effect, galaxy two-point correlation and luminosity functions, and the number densities of quasars and so on.

Large scale biasing effect can also be applied to various cosmological models beyond the CDM model. It will be interesting to investigate the difference in the amount of the biasing effect among various cosmological models. It will give an theoretical explanation to the observed geometric distribution of large-scale structure.

Finally we conclude that we have developed promising analytical frameworks which will enable us to study the large-scale structure of the universe more accurately than before.

Reproduced with permission of the copyright owner. Further reproduction prohibited without permission.

References

Adeva, B. et al. 1989, Phys. Lett., B231, 509

Arnol'd, V. I., Shandarin, S. F., & Zel'dovich, Ya. B. 1982, Geophys. Astrophys. Fluid Dynamics, 20, 111

Audit, E., & Alimi, J. M. 1996, A& A 315, 11

Audit, E., Teyssier, R., & Alimi, J. M. 1997, A& A, 325, 439

Bardeen, J. M., Bond, J. R., Kaiser, N., & Szalay, A. S. 1986, ApJ, 304, 15

Bahcall, N. A., & Cen, R. 1993, ApJ, 407, L49

Bahcall, N. A., & Fan, X. 1998, preprint astro-ph/980327

Bahcall, N. A., & Soneira, R. 1984, ApJ, 277, 27

Bernardeau, F. 1994, ApJ, 427, 51

Bond, J. R., Cole, S., Efstathiou, G., & Kaiser, N. 1991, ApJ, 379, 440

Bond, J. R., & Myers, S. T. 1996, ApJS, 103, 1

Brainerd, T. G., & Villumsen, J. V. 1992, ApJ, 394, 409

Bower, R. J., MNRAS, 248, 332

Buryak, O. E., Demianski, M., & Doroshkevich, A. G. 1992, ApJ, 393, 464

Carlberg, R. G., & Couchman, H. M. P. 1989, ApJ, 340, 47

Cavaliere, A., & Menci, N. 1993, ApJ, 407, L9

Cavaliere, A., & Menci, N. 1994, ApJ, 435, 528

Cavaliere, A., Menci, N., & Tozzi, P. 1996, ApJ, 464, 44

Cole, S., & Kaiser, N. 1998, MNRAS, 233, 637

Cole, S., & Kaiser, N. 1998, MNRAS, 237, 1127

Davis, M., Efstathiou G., Frenk C. S., & White, S. D. M., 1985, ApJS, 57, 241

Doroshkevich, A. G. 1967, Astrofizika, 3, 175

Doroshkevich, A. G. 1970, Astrofizika, 6, 581

Efstathiou, G., Frenk, C. S., White, S. D. M., & Davis, M. 1988, MNRAS, 235,

Reproduced with permission of the copyright owner. Further reproduction prohibited without permission.

715

Efstathiou, G., & Rees, M. J. 1988, MNRAS, 230, 5p

Eke, V., Cole, S., & Frenk, C. 1996, MNRAs, 283, 263

Fan, X., Bahcall, N. A., & Cen, R., 1997, ApJ, 490, L123

Girardi, M., Giuricin, G., Mardirossian, F., Mezzetti, M., & Boschin, W. 1998, preprint astro-ph/9804187

Governato, F., Babul, A., Quinn, T., Tozzi, P., Baugh, C. M., katz, N., & Lake, G. 1998, preprint astro-ph/9810189

Guth, A. H. 1981, Phys. Rev., D23, 347

Gelmini, G. 1990, in Dark Matter in the Universe, ed. P. Galeotti & D. N. Schramm (Denmark: Kluwer), 25

Gross, M. A. K., Somerville, R. S., Primack, J. R., Holtzman, J., & Klypin, A. 1997, preprint astro-ph/9712142

Hubbles, E. 1929, Proc. Natl. Acade. Sci, 15, 168

Jedamzik, K. 1995, ApJ, 448, 1

Kaiser, N. 1984, ApJ, 284, L9

Katz, N., Quinn, T., & Gelb, J. M. 1993, MNRAS, 265, 689

Kauffmann, G., & White, S. D. M., & Guiderdoni, B. 1993, MNRAS, 264, 201

Kofman, L., Bertschinger, E., Gelb, J. M., Nusser, A., & Dekel, A. 1994, ApJ, 420, 44

Kitayama, T., & Suto, Y. 1997, ApJ, 490, 557

Klypin, A., Borgani, S., Holtzman, J., & Primack, J. 1995, ApJ, 444, 1

Klypin, A. & Rhee, G. 1994, ApJ, 428, 399

Kolb, E. W., & Turner, M. S. 1990, The Early Universe (New York: Addison-Wesley)

Kuhlman, B., Melott, A. L., & Shandarin, S. F. 1996, ApJ, 470, L41

Lacey, C. & Cole, S. 1994, MNRAS, 271, 676

Lee, J. & Shandarin, S.F. 1998, ApJ, 500, 14

Reproduced with permission of the copyright owner. Further reproduction prohibited without permission.

Lachieze-Rey, M. 1995, Cosmology (Cambridge: Univ. of Chicago Press)

Lewis, A. D., Ellingson, D., Morris, S. L., Carlberg, R. G., preprint astro-ph/9901062

Linde, A. D., 1982, Phys. Lett., B108, 389

Linde, A. D., 1990, Inflation and Quantum Cosmology (Boston: Academic Press)

Lubin, P. M., & Villela, T. 1989, in The Cosmic Background Radiation and Fundamental Physics, ed. F. Melchiorri (Bologna: Editrice Compositore), 65

Lucchin, F. 1988, in Morphological Cosmology, ed. P. Flin & H. W. Duerbeck (Berlin: Springer), 284

Madsen, S., Doroshkevich, A. G., Gottlober, S., & Muller, V. 1997, preprint astro-ph/9709099

Melott, A. L., Sathyaprakash, B. S., & Sahni, V. 1996, ApJ, 456, 65

Shandarin, S. F. 1994, Physica D, 77, 342

Mo, H. J., & White, S. D. M., 1996, MNRAS, 282, 347

Monaco, P. 1995, ApJ, 447, 23

Monaco, P. 1998, Fundamentals of Cosmic Physics, 19, 157

Narayan, R., & White, S. d. M. 1988, MNRAS, 231, 97p

Oukbir, J., & Blanchard, A. 1992, A& A, 262, 210

Padmanabhan, T. 1993, Structure formation in the Universe (Cambridge: Cambridge Univ. Press)

Pagel, E. J. 1991, Phys. Scripta, T36, 7

Pauls, J. & Melott, A. L. 1995, MNRAS, 274, 99

Peacock, J., & Dodds, S. J. 1994, MNRAS, 267, 1020

Peacock, J. A., & Heavens, A. F. 1990, MNRAS, 243, 133

Peebles, P. J. E. 1980, the Large Scale Structure of the Universe, (Princeton: Princeton Univ. Press)

Peebles, P. J. E. 1982, ApJ, 258, 415

Peebles, P. J. E. 1985, ApJ, 297, 350

Peebles, P. J. E. 1990, ApJ, 365, 27

Reproduced with permission of the copyright owner. Further reproduction prohibited without permission.

Peebles, P. J. E., Schramm, D. N., Turner, E. L., & Kron, R. G. 1991, Nature, 352, 769

Peebles, P. J. E. 1993, Principles of Physical Cosmology (Princeton: Princeton Univ. Press)

Penzias, A. A., & Wilson, R. W. 1965, ApJ, 142, 419

Press, W. H., & Schechter, P. 1974, ApJ, 187, 425

Press, W. H., Teukolsky, S. A., Vetterling, W. T., & Flannery, B. P. 1992, Numerical Recipes in Fortran (Cambridge : Cambridge Univ. Press)

Robinson, J., Gawiser, E., & Silk, J. 1998, preprint astro-ph/9805181

Sahni, V., Sathyaprakash, B. S., & Shandarin, S. F. 1994, ApJ, 431, 20

Sandage, A. L. 1999, Invited Talk given at the Pritzker Symposium & Workshop on the Inflationary Universe

Shandarin, S.F. 1993, in Cosmic Velocity Fields, eds. F.R. Bouchet and M. Lachieze-Rey (Paris : Editions Frontieres), p. 383

Shandarin, S. F., & Klypin, A. A. 1984, Sov. Astron., 28, 491

Shandarin, S. F., Melott, A. L., McDavitt, K., Pauls, J. L., & Tinker, J. 1995, Phys. Rev. Lett., 75, 7

Shandarin, S. F., & Zel'dovich, Ya. B. 1989, Rev. Mod. Phys., 61, 185

Shaprio, P. R., Iliev, I., & Raga, A. C. 1998, preprint astro-ph/9810164

Sheth, R. K., & Tormen, G. 1999, preprint astro-ph/9901122

Silk, J., & White, S. D. 1978, ApJ, 223, L59

Smoot, G., F. 1999, preprint astro-ph/9902027

Sunyaev, R. A., & Zel'dovich, Y. B. 1970, Astrophys. and Sp. Sci. 7, 3

Tormen, G. 1998, preprint astro-ph/9802290

Tully, R. B., Scaramella, R., Vettolani, G., & Zamorani, G. 1992, ApJ, 388, 9

Van de Weygaert, R. & Babul, A. 1994, ApJ, 425, L59

Vergassola, M., Dubrulle, B., Frisch, U., & Noullez, A. 1994, A& A, 289, 325

Viana, P., & Liddle, R. 1996, MNRAS, 281, 323

Reproduced with permission of the copyright owner. Further reproduction prohibited without permission.

Wang, L. & Steinhardt, P.J. 1998, preprint astro-ph/9804015

White, S. D. M., & Frenk., C. S. 1991, ApJ, 379, 25

White, S. D. M., 1994, unpublished

Williams, B. G., Heavens, A. F., Peacock, J. A., & Shandarin, S. F. 1991, MNRAS, 250, 458

Yang, J., Schramm, D., Steigman, G., & Rood, R. T. 1979, ApJ, 227 , 697

Yano, T., Nagashima, M., & Gouda, N. 1996, ApJ, 466, 1

Zel'dovich, Ya. B. 1970, A& A, 5, 84

Yess, D. C., & Shandarin, S. F. 1996, ApJ, 465, 2

Reproduced with permission of the copyright owner. Further reproduction prohibited without permission.

Appendix A

Derivation of $p(\lambda_1)$, $p(\lambda_2)$, and $p(\lambda_3)$

In 1970 Doroshkevich found the joint probability distribution, $p(\lambda_1, \lambda_2, \lambda_3)$ of an ordered set of eigenvalues [equation (3.7) in § 3.2], corresponding to a Gaussian potential. In this appendix, we sketch the derivation of $p(\lambda_1)$, $p(\lambda_2)$, and $p(\lambda_3)$ [equation (3.8), (3.9) and (3.10) in § 3.2], and investigate their statistical properties.

The two point probability distributions, $p(\lambda_1, \lambda_2), p(\lambda_2, \lambda_3)$ and $p(\lambda_1, \lambda_3)$ can be easily obtained from the direct integration of $p(\lambda_1, \lambda_2, \lambda_3)$ such that

$$\begin{aligned} p(\lambda_1, \lambda_2) &= \int_{-\infty}^{\lambda_2} p(\lambda_1, \lambda_2, \lambda_3) d\lambda_3 \\ &= \frac{1125}{64\sqrt{5}\pi\sigma^4}\Bigg\{(\lambda_1 - \lambda_2)(3\lambda_1 - \lambda_2)\exp\Big[-\frac{3\lambda_1^2}{\sigma^2} + \frac{3\lambda_1\lambda_2}{\sigma^2} - \frac{9\lambda_2^2}{2\sigma^2}\Big] \\ &\quad + \frac{\sqrt{3\pi}\sigma}{12}(\lambda_1 - \lambda_2)\Big[8 + \frac{3}{\sigma^2}(3\lambda_1 - \lambda_2)(3\lambda_2 - \lambda_1)\Big] \\ &\quad \times \exp\Big[-\frac{45\lambda_1^2}{16\sigma^2} + \frac{15\lambda_1\lambda_2}{8\sigma^2} - \frac{45\lambda_2^2}{16\sigma^2}\Big]\mathrm{erfc}\Big[\frac{\sqrt{3}}{4\sigma}(\lambda_1 - 3\lambda_2)\Big]\Bigg\}, \quad \text{(A.1)} \end{aligned}$$

$$\begin{aligned} p(\lambda_2, \lambda_3) &= \int_{\lambda_2}^{\infty} p(\lambda_1, \lambda_2, \lambda_3) d\lambda_1 \\ &= \frac{1125}{64\sqrt{5}\pi\sigma^4}\Bigg\{(\lambda_2 - \lambda_3)(\lambda_2 - 3\lambda_3)\exp\Big[-\frac{3\lambda_3^2}{\sigma^2} + \frac{3\lambda_2\lambda_3}{\sigma^2} - \frac{9\lambda_2^2}{2\sigma^2}\Big] \end{aligned}$$

Reproduced with permission of the copyright owner. Further reproduction prohibited without permission.

$$+\frac{\sqrt{3\pi}\sigma}{12}(\lambda_2-\lambda_3)\Big[8+\frac{3}{\sigma^2}(\lambda_2-3\lambda_3)(\lambda_3-3\lambda_2)\Big]$$
$$\times\exp\Big[-\frac{45\lambda_2^2}{16\sigma^2}+\frac{15\lambda_2\lambda_3}{8\sigma^2}-\frac{45\lambda_3^2}{16\sigma^2}\Big]\mathrm{erfc}\Big[\frac{\sqrt{3}}{4\sigma}(3\lambda_2-\lambda_3)\Big]\Big\}, \quad \text{(A.2)}$$

$$\begin{aligned}
p(\lambda_1,\lambda_3) &= \int_{\lambda_3}^{\lambda_1} p(\lambda_1,\lambda_2,\lambda_3)d\lambda_2 \\
&= \frac{1125}{64\sqrt{5}\pi\sigma^4}\Big\{(\lambda_1-\lambda_3)(3\lambda_1-\lambda_3)\exp\Big[-\frac{3\lambda_1^2}{\sigma^2}+\frac{3\lambda_1\lambda_3}{\sigma^2}-\frac{9\lambda_3^2}{2\sigma^2}\Big] \\
&\quad +(\lambda_1-\lambda_3)(\lambda_1-3\lambda_3)\exp\Big[-\frac{3\lambda_3^2}{\sigma^2}+\frac{3\lambda_1\lambda_3}{\sigma^2}-\frac{9\lambda_1^2}{2\sigma^2}\Big] \\
&\quad +\frac{\sqrt{3\pi}\sigma}{12}(\lambda_1-\lambda_3)\Big[\frac{3}{\sigma^2}(3\lambda_1-\lambda_3)(\lambda_1-3\lambda_3)-8\Big] \\
&\quad \times\exp\Big[-\frac{45\lambda_1^2}{16\sigma^2}+\frac{15\lambda_1\lambda_3}{8\sigma^2}-\frac{45\lambda_3^2}{16\sigma^2}\Big] \\
&\quad \times\Big\{\mathrm{erfc}\Big[\frac{\sqrt{3}}{4\sigma}(3\lambda_1-\lambda_3)\Big]-\mathrm{erfc}\Big[\frac{\sqrt{3}}{4\sigma}(3\lambda_3-\lambda_1)\Big]\Big\}\Big\} \qquad \text{(A.3)}
\end{aligned}$$

In order to derive $p(\lambda_1)$, $p(\lambda_2)$, and $p(\lambda_3)$, we have to integrate the above two point distributions, which involve complex error function terms as one can see. We find the following recursion formula which is useful in integrating such complex terms.

$$\begin{aligned}
\int t^n\exp(-a^2t^2)\mathrm{erf}(\mathrm{bt})dt &= \frac{n-1}{2a^2}\int t^{n-2}\exp(-a^2t^2)\mathrm{erf}(\mathrm{bt})dt \\
&\quad -\frac{1}{2a^2}t^{n-1}\exp(-a^2t^2)\mathrm{erf}(\mathrm{bt}) \\
&\quad +\frac{b}{a^2\sqrt{\pi}}\int t^{n-1}\exp[-(a^2+b^2)t^2]dt. \qquad \text{(A.4)}
\end{aligned}$$

With the above recursion formula, it is straightforward to derive the individual distributions. The results are shown in § 3.2.

Reproduced with permission of the copyright owner. Further reproduction prohibited without permission.

Appendix B

Derivation of $P(M, M')$

In the framework of our formalism, the conditional probability $P(M, M')$ is written as

$$P(M, M') = P(\lambda_3 > \lambda_{3c} | \lambda_3' = \lambda_{3c}) = \frac{P(\lambda_3 > \lambda_{3c}, \lambda_3' = \lambda_{3c})}{P(\lambda_3' = \lambda_{3c})}, \qquad \text{(B.1)}$$

where λ_3 and λ_3' are the lowest eigenvalue of the deformation tensor at the same point but at two different filtering mass scale M and M' respectively.

In order to derive the probability $P(\lambda_3 > \lambda_{3c}, \lambda_3' = \lambda_{3c})$, we start with the multivariate Gaussian joint probability distribution (see Doroshkevich 1970; Bardeen et al. 1986) for the six independent elements of the deformation tensor at two different mass scales:

$$p_J(y_1, \cdots, y_6') dy_1 \cdots dy_6' = \frac{\exp(-Q)}{(2\pi)^6 \sqrt{\det(V)}} dy_1 \cdots dy_6', \qquad \text{(B.2)}$$

$$Q = \frac{1}{2} \mathbf{y}^{\mathbf{t}} \cdot V \cdot \mathbf{y} \qquad \text{(B.3)}$$

Here V is the covariance matrix, while $\{y_i\}_{i=1}^6$ and $\{y_1'\}_{i=1}^6$ are the six independent elements of the deformation tensor (defined by equation (3.6) in § 3.2; $y_1 \equiv d_{11}$, $y_2 \equiv d_{22}$, $y_3 \equiv d_{33}$, $y_4 \equiv d_{12}$, $y_5 \equiv d_{23}$, $y_6 \equiv d_{31}$) at mass scale M and M' respectively.

Reproduced with permission of the copyright owner. Further reproduction prohibited without permission.

In the case of a sharp k-space filter, the mutual correlations between $\{y_i\}_{i=1}^6$ and $\{y_1'\}_{i=1}^6$ are

$$< y_i^2 >= \frac{\sigma_M^2}{5}, \qquad < y_i y_j >= \frac{\sigma_M^2}{15}, \qquad < y_i y_i' >= \frac{\sigma_{M'}^2}{5}, \tag{B.4}$$

$$< y_i'^2 >= \frac{\sigma_{M'}^2}{5}, \qquad < y_i' y_j' >= \frac{\sigma_{M'}^2}{15}, \qquad < y_i y_j' >= \frac{\sigma_{M'}^2}{15}, \tag{B.5}$$

for $i, j(\neq i) = 1, 2, 3$, and

$$< y_i^2 >= \frac{\sigma_M^2}{15}, \qquad < y_i y_j >= 0, \qquad < y_i y_i' >= \frac{\sigma_{M'}^2}{15}, \tag{B.6}$$

$$< y_i'^2 >= \frac{\sigma_{M'}^2}{15}, \qquad < y_i' y_j' >= 0, \qquad < y_i y_j' >= 0, \tag{B.7}$$

for $i, j(\neq i) = 4, 5, 6$. Here σ_M^2 and $\sigma_{M'}^2$ are the mass variance of the density field filtered at the mass scale M and M' respectively.

Through equations (B2) to (B7), along with the similarity transformation of the deformation tensor into its principal axes, we find the following joint probability distribution of the three eigenvalues $\{\lambda_i\}_{i=1}^3$, $\{\lambda_i'\}_{i=1}^3$ of the deformation tensor at filtering mass scale M, M' $(M \ll M')$ respectively.

$$\begin{aligned} p_J(\lambda_1, \cdots, \lambda_3')d\lambda_1 \cdots d\lambda_3' \;\approx\; & p_{J1}(\Delta_1, \Delta_2, \Delta_3)d\Delta_1 d\Delta_2 d\Delta_3 \\ & \times p_{J2}(\lambda_1', \lambda_2', \lambda_3')d\lambda_1' d\lambda_2' d\lambda_3' \end{aligned} \tag{B.8}$$

$$p_{J1} = \frac{5^3 \cdot 3^3}{2^4 \pi^3 \sigma_\Delta^6 \sqrt{5}} \exp\left[-\frac{3I_1^2}{\sigma_\Delta^2} + \frac{15I_2}{2\sigma_\Delta^2} \right] (\Delta_1 - \Delta_2)(\Delta_2 - \Delta_3)(\Delta_3 - \Delta_1) \tag{B.9}$$

$$p_{J2} = \frac{5^3 \cdot 3^3}{2^4 \pi^3 \sigma_{M'}^6 \sqrt{5}} \exp\left[-\frac{3I_1'^2}{\sigma_{M'}^2} + \frac{15I_2'}{2\sigma_{M'}^2} \right] (\lambda_1' - \lambda_2')(\lambda_2' - \lambda_3')(\lambda_3' - \lambda_1') \tag{B.10}$$

where

$$\Delta_i \equiv \lambda_i - \lambda_i', \qquad \sigma_\Delta^2 \equiv \sigma_M^2 - \sigma_{M'}^2, \tag{B.11}$$

Reproduced with permission of the copyright owner. Further reproduction prohibited without permission.

$$I_1 \equiv \Delta_1 + \Delta_2 + \Delta_3, \qquad I_2 \equiv \Delta_1\Delta_2 + \Delta_2\Delta_3 + \Delta_3\Delta_1, \tag{B.12}$$

$$I_1' \equiv \lambda_1' + \lambda_2' + \lambda_3', \qquad I_2' \equiv \lambda_1'\lambda_2' + \lambda_2'\lambda_3' + \lambda_3'\lambda_1'. \tag{B.13}$$

Note the similarity between p_{J1} and p_{J2}. In fact the above equations hold good only in the case of a sharp k-space filter.

The integration of p_J over $\lambda_1, \lambda_2, \lambda_1'$, and λ_2' gives us the joint probability density distribution, $p(\lambda_3, \lambda_3')$:

$$p(\lambda_3, \lambda_3')d\lambda_3 d\lambda_3' = p(\Delta_3)d\Delta_3 p(\lambda_3')d\lambda_3'. \tag{B.14}$$

Here the probability density distributions of $p(\Delta_3)$ and $p(\lambda_3')$ have the same form as $p(\lambda_3)$ [equation (3.10)] except for the value of the variance.

Finally we derive the conditional probability $P(M, M')$:

$$\begin{aligned} P(M, M') &\approx \frac{P(\lambda_3 > \lambda_{3c}, \lambda_3' = \lambda_{3c})}{P(\lambda_3' = \lambda_{3c})} = \frac{p(\lambda_3' = \lambda_{3c})d\lambda_3' \int_0^\infty d\Delta_{3c} p(\Delta_{3c})}{p(\lambda_3' = \lambda_{3c})d\lambda_3'} \\ &= \int_0^\infty d\Delta_{3c} p(\Delta_{3c}) = \int_0^\infty d\lambda_3 p(\lambda_3) = 0.08\Theta(M' - M), \end{aligned} \tag{B.15}$$

where Δ_{3c} is $\lambda_3 - \lambda_{3c}$.

Reproduced with permission of the copyright owner. Further reproduction prohibited without permission.